OLD DOMINION UNIVERSITY RESEARCH FOUNDATION

Contract NAS9-13410
DRL No. T-897
DRD No. MA-183T
NASA CR.
144400

SCHOOL OF ENGINEERING
OLD DOMINION UNIVERSITY
NORFOLK, VIRGINIA

Technical Report 75-T6

EXPERIMENTAL AND ANALYTICAL INVESTIGATION OF "0" G CONDENSATION IN A MECHANICAL REFRIGERATION SYSTEM APPLICATION

By

Edward G. Keshock

May 1975

Prepared for the
National Aeronautics and Space Administration
Lyndon B. Johnson Space Center
Houston, Texas

Contract NAS9-13410
DRL No. T-897
DRD No. MA-183T

SCHOOL OF ENGINEERING
OLD DOMINION UNIVERSITY
NORFOLK, VIRGINIA

Technical Report 75-T6

EXPERIMENTAL AND ANALYTICAL INVESTIGATION OF "0" G CONDENSATION IN A MECHANICAL REFRIGERATION SYSTEM APPLICATION

By
Edward G. Keshock

May 1975

Prepared for the
National Aeronautics and Space Administration
Lyndon B. Johnson Space Center
Houston, Texas 77058

Submitted by the
Old Dominion University Research Foundation
Norfolk, Virginia 23508

DISTRIBUTION

	Copies
NASA Lyndon B. Johnson Space Center R&T Procurement Branch Attn: Tommy McPhillips, Mail Code BC72 Houston, TX 77058	1
NASA Lyndon B. Johnson Space Center Technical Library Branch Attn: Retha Shirkey, Mail Code JM6 Houston, TX 77058	4
NASA Lyndon B. Johnson Space Center Management Services Division Attn: John T. Wheeler, Mail Code JM7 Houston, TX 77058	1
NASA Lyndon B. Johnson Space Center Environmental and Thermal Systems Section Attn: Burrell O. French/EC2 Houston, TX 77058	10
Dr. John A. Weese Dean, School of Engineering Old Dominion University Norfolk, VA 23508	1
Dr. Edward G. Keshock School of Engineering Old Dominion University Norfolk, VA 23508	7
Old Dominion University Research Foundation Norfolk, VA 23508	1
Total	25

ABSTRACT

Basic equations of momentum and energy are presented and discussed with respect to heat transfer and pressure drop for forced flow condensation in horizontal tubes under 1-g and 0-g conditions. Some experimental results are presented for condensing refrigerant-12 in a system of three parallel-connected quartz tubes (3-mm inside diameter, G = 1.037 to 3.456 x 10^5 lbm/hr-ft^2). From high speed photographs measurements were obtained of film thickness, phase velocities, disturbance wavelengths, and flow regimes and their transitions. Based upon these measurements various dimensionless force ratios (flow and instability parameters) were calculated. Under 0-g conditions a uniformly thick redistribution of liquid condensate about the tube walls was found to result in a lowered heat transfer coefficient as compared with 1-g conditions, based upon fundamental heat transfer theory. A model is proposed that takes into account the difference in heat transfer due to condensate distribution under 1-g and 0-g conditions.

CONTENTS

LIST OF TABLES

LIST OF FIGURES

LIST OF FIGURES (concl'd.)

NOMENCLATURE

A	area, or total cross-sectional flow area (liquid plus vapor)
c_p	specific heat
D	diameter
dE	dissipation of mechanical energy into heat per unit mass
F	force exerted in overcoming friction
F_o	wall shear stress, having components due to gravity, momentum, and friction, as defined in equation (44)
F_1	$F_o\, g_c/g(\rho_\ell - \rho_v)(\nu_\ell/g)^{1/3}$
F_2	defined in equations (36a), (36b), (36c)
F_2'	defined in equation (31)
f	friction factor
g	acceleration due to gravity
g_c	gravitational constant
G, G_T	total mass flow rate per unit area
h, h_z	local heat transfer coefficient
h_m	mean heat transfer coefficient
h_c	convective heat transfer coefficient
h_{ow}	heat transfer coefficient on outer wall
i	enthalpy
k	thermal conductivity
L	axial distance
M	Mach number
p, P	pressure
Pr	Prandtl number
q	heat transfer rate
δ_q	heat absorbed from surroundings

r_f	dimensionless friction multiplier for an unheated pipe
r_g	dimensionless gravity multiplier for an unheated pipe
R	channel radius
ΔR	incremental radial distance
S	force exerted by vapor on liquid at interface
St_z^*	local Stanton number, $h_z/\rho_\ell\ c_p\ u_\tau$
T,t	temperature
u	velocity
U	overall heat transfer coefficient
v	specific volume
V	velocity
W, W_T	total mass rate of flow (liquid plus vapor)
W_f, W_g	mass flow rates of liquid and vapor phases
δ_w	work done on surroundings
x	quality
X	Lockhart-Martinelli parameter
X_{tt}	defined by equation (57b)
y^+	dimensionless distance from wall, $y\ u_\tau/v_\ell$
z	axial coordinate

Greek Symbols

α	void fraction
γ	specific heat ratio
Γ	liquid flow rate per unit circumference; also used as grouping symbol, equation (62b)
δ	liquid film thickness
δ^+	dimensionless film thickness, $\delta\ u_\tau/\nu_\ell$

δ_{act}	actual film thickness about tube periphery
δ_{obs}	film thickness measured (observed) at tube bottom
θ	angle of inclination of flow system with the horizontal
λ	latent heat of vaporization
λ_c	critical wavelength
λ_d	most dangerous wavelength
$\lambda_{d,mod}$	modified most dangerous wavelength due to curvature of liquid-vapor interface
μ	dynamic viscosity
ν	kinematic viscosity
ρ	density
$\overline{\rho}$	mixture density, $\rho_f (1 - \alpha) + \rho_g (\alpha)$
σ	surface tension
τ_v	vapor shear stress on the liquid film
ϕ_v^2	pressure drop multiplier (see equation 23)

Subscripts

a	accelerational component
e	exit
f	liquid
F	frictional component of pressure drop
F,g	frictional component of pressure drop, vapor phase
F,f	frictional component of pressure drop, liquid phase
g	vapor phase
g	gravitational component
i,IN	inlet conditions (also refers to interface in eqs. (44), (54), (55)
ℓ	liquid phase

ℓv	difference, liquid and vapor phases
m	mean value
M	momentum component
o	inlet conditions
sup	superheated conditions
s,sat	saturation conditions
T	total
w	wall conditions
z	axial position

EXPERIMENTAL AND ANALYTICAL INVESTIGATION OF "O" G CONDENSATION IN A MECHANICAL REFRIGERATION SYSTEM APPLICATION

By

Edward G. Keshock[1]

INTRODUCTION

General Description

This study is part of an effort to develop a mechanical refrigeration system that can be used in advanced spacecraft. Thermodynamic considerations make it highly desirable for the refrigeration system to reject heat directly from the condenser, rather than by transferring heat directly from the condenser to an intermediate fluid loop that rejects heat from a conventional space radiator. Thus the need exists to develop a condenser/radiator system that functions both as a conventional space radiator and as a condenser in a refrigeration cycle. This could result in a reduction of external area requirements for the spacecraft heat rejection system, which would be quite desirable.

However, before employing such a system in a spacecraft, questions arise as to whether or not the system will function suitably in a zero-g environment. That is, while one-g system tests may provide much useful information regarding the operational characteristics of the system, such tests leave unanswered several questions regarding zero-g operational capabilities. Specifically, the two-phase flow that occurs in the radiator/condenser (r/c) panel of such a refrigeration system must be understood with

---

[1] Associate Professor of Engineering, Old Dominion University, Norfolk, Virginia 23508.

respect to heat transfer, pressure drop, stability, and liquid-vapor separation characteristics under conditions of zero-gravity. Consequently, it was decided that testing such a system in a simulated zero-g environment, using a KC-135 aircraft, was necessary to further such understanding.

The present study contains both experimental and analytical aspects of the two-phase flow condensation characteristics of one component of the overall refrigeration-heat rejection system, an r/c panel, whose design is described in detail elsewhere (refs. 1-3). It was originally intended that operational data of the r/c panel be obtained under both 1-g and 0-g conditions to form the basis of this study. However, no quantitative zero-g data was obtained, and so the conclusions presented herein cannot be directly verified by experimental results.

Previous Zero-G Investigations

One of the earliest investigations of condensing processes in zero-gravity conditions was conducted by Feldmanis (ref. 4), who made temperature, pressure, and photographic measurements of forced convection condensation of distilled water in a single, tapered, tube, with a 1.74 cm inlet i.d. He reported an increase in condensate temperature during low gravity conditions that may have been caused by reduced condensation heat transfer coefficients, possibly attributable to the absence of gravity forces acting to remove the condensate film from the cooled surface within the tube.

Two studies of significance, investigating the flow condensation of a non-wetting fluid (mercury) in tubes, were conducted by Albers and Macosko (ref. 5) and Namkoong, et al. (ref. 6); both studies employed a Navy AJ-2 bomber flying a Keplerian trajectory to attain the 0-g environment. Tube sizes ranged from 0.686 to 1.245 cm i.d. Namkoong, et al. (ref. 6) reported a concentration of drops on the tube bottom and a shallow sloping interface under 1-g conditions, while in a 0-g environment the drops were uniformly distributed and the interface was vertical. Albers and Macosko reported that (1) measured overall static pressure drops at two mass flow rates

were essentially the same for 1- and 0-g conditions, and (2) the Lockhart-Martinelli parameter ϕ_g and two-phase flow pressure gradient were affected negligibly by gravity, as also were the fog-flow correlations.

In the study related most closely to the present one, Soliman and Berenson (ref. 7) studied flow condensation of Freon-113 in a transparent multi-tube condenser. Both tapered and constant-diameter tubes were studied, the latter containing twisted tape and wire in some cases. Tube diameters ranged from 0.335 to 0.595 cm i.d. The gravitational effects studied, however, were those attained from operating the condenser in positions ranging from a +90-degree position (condensing downwards) to a -90-degree position (condensing upwards).

In a study of wetting and non-wetting mercury condensation (ref. 8) fluoroscopic observations indicated a fog-flow regime terminated by a rather elongated sloping interface at the "point" of complete condensation. Their observation of the non-wetting flow indicated a predominantly fog-flow regime with some droplets at the walls, terminated by a more or less vertical, distinct interface [see also (refs. 5,6)]. These observations led to their employment of a fog-flow model for predicting pressure drop.

Present Objectives

The broad objective of the present study was to obtain, analyze and interpret operational data, obtained in 1-g and 0-g environments, of the radiation/condenser panel (described in Experimental Procedures), so as to form the basis for and/or verify analytical results that would be capable of predicting zero-g behavior of other flow condensation systems generally. The specific type of operational data referred to is that related to heat transfer, pressure drop, and flow stability in the parallel flow channel system.

In order to accomplish the preceding, a secondary objective was created--that of obtaining and analyzing photographic infor-

mation of the two-phase flow characteristics in a transparent multi-tube flow system that modelled the flow characteristics of the full-size r/c panel.

From such data, and from theoretical predictions, it was desired to establish parameters of significance in scaling 1-g results (operational characteristics) to 0-g conditions, and the functional dependencies of such parameters in predicting flow condensation behavior with respect to pressure drop, heat transfer, and stability, in 0-g environments.

As indicated earlier, no quantitative 0-g data was obtained, so that no verification of predicted behavior is possible here.

THEORY

Basic Equations

The model utilized here, shown in figure 1, is that of a stratified single component flow in an inclined tube, allowing mass transfer between the phases, as in reference 9. The flow is assumed to be steady, and there are no variations of properties in any plane normal to the flow. The velocity and density of each phase are mean values at any particular axial location (constant across the plane). The pressure is also assumed constant across the plane normal to the flow.

Conservation of mass.- In the absence of the addition or removal of mass through channel walls, the equations expressing the conservation of mass are:

$$W_g + W_f = W \tag{1}$$

$$dW_g = -dW_f \tag{2}$$

$$W_g = \rho_g A_g u_g = Wx \tag{3}$$

$$W_f = \rho_f A_f u_f = W(1 - x) \tag{4}$$

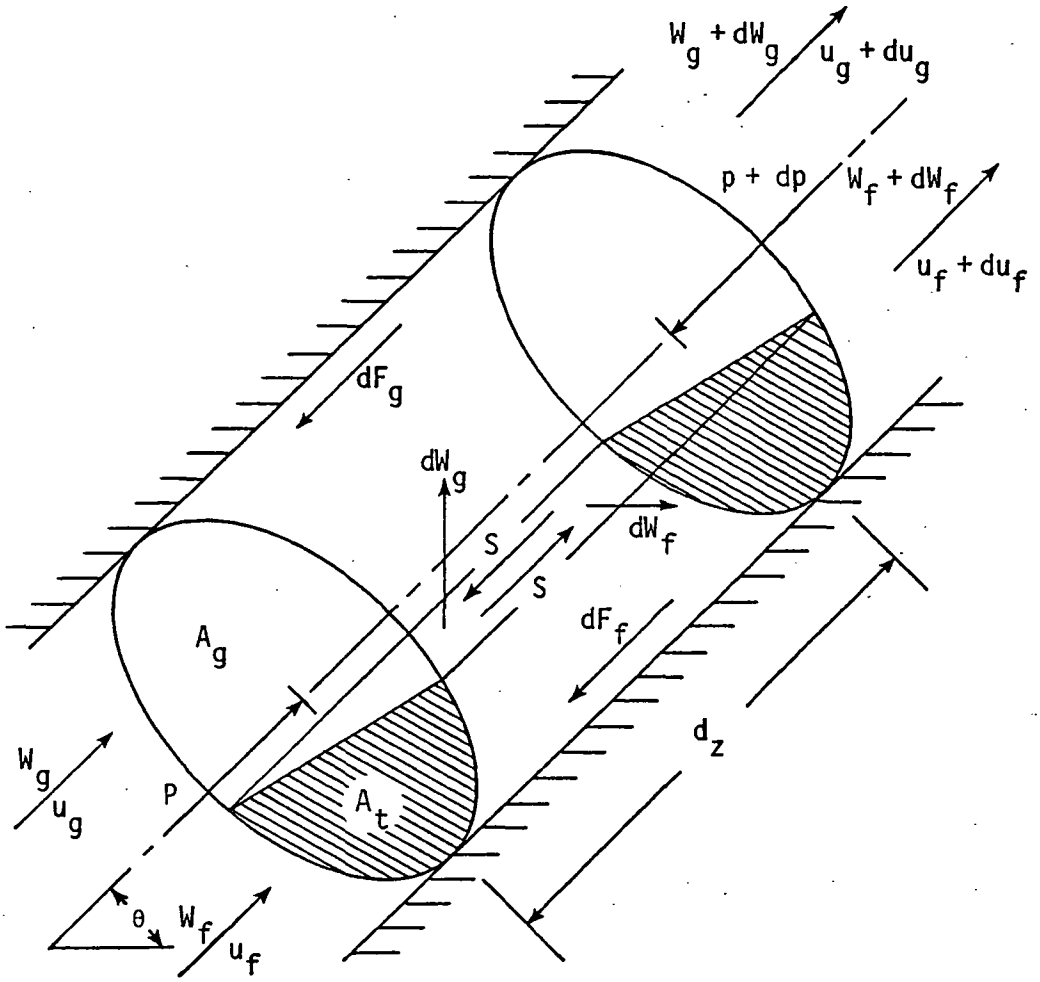

Figure 1. Simplified model for two-phase flow over element of channel (ref. 9).

$$\frac{d}{dz}(\rho_g A_g u_g) = W\frac{dx}{dz} = \frac{dW_g}{dz} \tag{5}$$

$$\frac{d}{dz}(\rho_f A_f u_f) = -W\frac{dx}{dz} = \frac{dW_f}{dz} \tag{6}$$

where the terms are pictured and defined in figure 1 and the nomenclature section.

Conservation of momentum.- Equating the forces acting on each phase to the rate of change of momentum of that phase, one obtains, first for the vapor phase,

$$pA_g - (p + dp)A_g - dF_g - S - A_g dz\rho_g g \sin\theta = \left[(W_g + dW_g)(u_g + du_g) - W_g u_g - dW_g u_f\right] \tag{7}$$

where dF_g and S are the forces exerted by the vapor phase in overcoming frictional resistance at the wall and at the liquid-vapor interface, respectively. Simplifying, one obtains

$$-A_g dp - dF_g - S - A_g dz\rho_g g \sin\theta = W_g du_g + dW_g u_g - dW_g u_f \tag{8}$$

Similarly, for the liquid phase,

$$-A_f dp - dF_f + S - A_f dz\rho_f g \sin\theta = W_f du_f \tag{9}$$

where S is now a force on the liquid. Adding (8) and (9), one obtains

$$-Adp - dF_g - dF_f - g\sin\theta\, dz\left[A_f\rho_f + A_g\rho_g\right] = d(W_f u_f + W_g u_g) \tag{10}$$

which is the basic differential momentum equation.

The frictional terms may be expressed in terms of the areas occupied by each phase (note that the model of figure 1 assumes no liquid layer or film covering the top inside surface of the channel, a condition that is likely not to exist under zero-g conditions) as follows:

$$(dF_g + S) = -A_g \left(\frac{dp}{dz}\right)_{F,g} dz \tag{11}$$

$$(dF_f - S) = -A_f \left(\frac{dp}{dz}\right)_{F,f} dz \tag{12}$$

Combining,

$$(dF_g + dF_f) = -A \left(\frac{dp}{dz}\right)_F dz \tag{13}$$

where $\left(\frac{dp}{dz}\right)_F$ represents that part of the overall static pressure gradient required to overcome friction. Substituting (13) into (10), one may obtain

$$\left(\frac{dp}{dz}\right) = \left(\frac{dp}{dz}\right)_F + \left(\frac{dp}{dz}\right)_a + \left(\frac{dp}{dz}\right)_z \tag{14}$$

or in terms of quality, void fraction, fluid densities, and mass flow rates, the latter two terms are evaluated to be

$$-\left(\frac{dp}{dz}\right)_a = \frac{1}{A} \frac{d}{dz} \left(W_g u_g + W_f u_f\right) \tag{15}$$

$$= G^2 \frac{d}{dz} \left[\frac{x^2 v_g}{\alpha} + \frac{(1 - x)^2}{(1 - \alpha)} v_f\right]$$

and

$$-\left(\frac{dp}{dz}\right)_z = g \sin \theta \left[\frac{A_g}{A} \rho_g \frac{A_f}{A} \rho_f\right]$$

$$= g \sin \theta \left[\alpha\rho_g + (1 - \alpha)\rho_f\right] \tag{16}$$

It should be observed that in a zero-g environment the contribution to the overall pressure drop due to static head, $\left(\frac{dp}{dz}\right)_z$, is zero, regardless of the orientation of the system (provided, of course, there is no appreciable rotation of the system also). Consequently, it should be expected that the pressure drop performance of a two-phase system is likely to improve in a zero-g environment, since it also seems likely that the acceleration and frictional components are at the same time likely to not increase.

It should also be observed that the accurate evaluation of the frictional pressure drop component in a zero-g environment may require the use of a model different from that in figure 1, since it is expected that for small diameter tubes, and flow rates similar to those experienced in this study, a continuous liquid film will exist on the wall, preventing a frictional resistance at a vapor-solid interface. Instead, only liquid-solid and liquid-vapor interfaces will be present, except, perhaps, only near the origin of the flow channel.

Conservation of energy.- Considering both phases together, the equation describing the conservation of total energy is

$$W(\delta q - \delta w) = W di + d\left[\frac{W_g u_g^2}{2} + \frac{W_f u_f^2}{2}\right] + W_g \sin \theta \, dz \tag{17}$$

For no net work on the surroundings ($\delta\omega = 0$), and where

$$di = \delta q + dE + \frac{dp}{W}\left[W_g v_g + W_f u_f\right] \tag{18}$$

and expressing in terms of more practical system parameters,

$$-\left(\frac{dp}{dz}\right)\left[xv_g + (1 - x)v_f\right] = \frac{dE}{dz} + \frac{G^2}{2}\frac{d}{dz}\left[\frac{x^3 v_g^2}{\alpha^2} + \frac{(1 - x)^3 v_f^2}{(1 - \alpha)^2}\right] + g \sin \theta \quad . \tag{19}$$

Again, it is observed that the total static pressure gradient is expressible in terms of a frictional dissipation term, an accelerational (kinetic) head term, and a static head term. However, the frictional term here also includes the dissipation of mechanical energy at the liquid-vapor interface due to the relative motion of the phases.

Both (16) and (19) indicate that there will be no static head contribution to the pressure gradient (and pressure drop) in a zero-g environment. If the acceleration and friction components remain approximately the same under both 1- and 0-g conditions (and it appears reasonable they will, judging from expectations of the flow hydrodynamics under both conditions), then pressure drop measurements in a horizontal orientation under 1-g conditions should provide reasonable and conservative expectations of pressure drops to be experienced under 0-g conditions.

Pressure Drop

General approaches.- The ultimate practical aim of most two-phase studies is to predict the heat transfer and pressure drop characteristics of two-phase systems analytically, i.e., without going to the great expense of modeling the system experimentally. Yet there are a variety of analytical techniques presently available, none of which are universally applicable or accurate. Whichever techniques may be employed, however, one of the fundamental objectives of the present study is to attempt to establish the differences in two-phase flow condensation systems in 1- and 0-g environments, and to develop techniques that will predict possible differences in heat transfer and pressure drop that may occur.

Regarding the general analytical techniques that have been applied to two-phase systems, three general approaches may be employed. They are (1) the homogeneous model, (2) the separated flow model, and (3) methods based on particular flow regimes.

The homogeneous model is the easiest to use, and is the most general. However, it is also the least accurate. Generally, the prediction of the pressure drop attributable to gravity, using the homogeneous model, is quite poor. "If the gravity pressure drop is very large, the homogeneous model will do a poor job of predicting the pressure drop" (ref. 10). On the other hand, the momentum pressure drop can be predicted with quite good results (ref. 10). Bubbly flow systems can often be described adequately by the homogeneous model.

In the separated flow model, the two methods most often employed are the Thom method and the Martinelli-Nelson method. The Thom method has supplanted the Martinelli method at high pressures, but at pressures near atmospheric for a wide variety of liquids, the Martinelli procedure is still the best. Both are based upon experimental data, though more so in the Thom method. The separated flow model improves upon the homogeneous model in that (1) the velocities of the two phases are allowed to differ, and (2) the friction factor is allowed to become a function of quality. Both of the preceding allowances portray the actual flow conditions more realistically.

The third method, the flow regime method, would hope to predict pressure drop, void fraction, and other quantities, for <u>each</u> flow regime occurring in the system, thus analyzing the total system with much greater accuracy and precision. However, two difficulties alone have deterred greater use of this method, namely (1) the regime boundaries are not distinct, so that the definition of boundaries are subjective, and to some extent arbitrary, and (2) the precision required is often not so great as to justify the complication involved in completely mapping and defining the flow patterns of the system. It is, on the other hand, useful to identify flow regimes if only to indicate limits on the range of validity of the

particular model employed. Also, phase "boundaries" are automatically identified, and order of magnitude calculations may be made, suggesting the variables that may be most worthwhile investigating further.

Separated flow model.- Using the separated flow model approach, and employing a modified Lockhart-Martinelli technique (ref. 11), the three components of pressure drop composing the total static pressure drop are given by

$$\left(\frac{dp}{dL}\right)_T = \left(\frac{dp}{dL}\right)_M + \left(\frac{dp}{dL}\right)_f + \left(\frac{dp}{dL}\right)_g \tag{20}$$

where

$$\left(\frac{dP}{dL}\right)_M = -\frac{2xW_T^2}{g_c \rho_v A_v^2} \frac{dx}{dL} \tag{21}$$

$$\left(\frac{dP}{dL}\right)_g = \bar{\rho} \frac{g}{g_c} \sin \theta \tag{22}$$

$$\left(\frac{dP}{dL}\right)_f = \phi_v^2 \left(\frac{dP}{dL}\right)_v \tag{23}$$

In (23), after the manner of Martinelli, et al. (refs. 12, 13),

$$\phi_v = \phi_v (X^2)$$

where

$$X = \frac{(dP/dL)_\ell}{(dP/dL)_v} .$$

It should be noted that in the gravitational pressure drop, the angle θ is measured from the horizontal. Consequently, the gravitational pressure drop is positive for upward flow, negative for downward flow, and zero for horizontal flow. This suggests, then, that condensing tests should be conducted with the apparatus

in a horizontal plane so as to minimize gravitational effects upon pressure drop. The gravitational pressure drop term need not be evaluated then.

Gravitational effects will not be eliminated completely, however, since the two-phase flow patterns will be affected to some extent by gravity, e.g., vapor bubbles moving near the top of the flow channel rather than in the center, as in a 0-g environment. Thus pressure drops may yet be modified somewhat from the 0-g values due to the influence of gravity in modifying flow patterns from those that would exist under 0-g conditions. For example, the frictional contribution to the pressure drop in the Thom method is presented in terms of a multiplier, i.e.,

$$\Delta P_f = 4f \frac{L}{D} \frac{G^2}{2g_c} v_f \quad r_f \tag{24}$$

where r_f is a function of both pressure and gravity.

If the effect of gravity is neglected, the total static pressure change due to momentum and two-phase friction is given by reference 11:

$$\Delta P_T = \left[C \frac{4fL}{D} - 2 \right] \frac{G_T^2}{2\rho_v g_c} \tag{25}$$

where C is a suitable factor used to multiply the one-phase frictional pressure drop to yield the two-phase frictional pressure drop. As stated in reference 11, however, C is a factor of physical properties and heat flux distribution that may require evaluation for every particular condensing system.

In the Thom method the momentum pressure drop for a system starting with saturated vapor at the entrance and having saturated liquid at the exit is also $(G_T^2/\rho_v g_c)$. The friction contribution to pressure drop is given by

$$\Delta P_f = 4f \frac{L}{D} \frac{G^2}{2\rho_f g_c} r_f \tag{26}$$

where r_f is a function of gravity and pressure for water, and f is the Moody friction factor assuming saturated water flowing at the mixture mass velocity (ref. 10). The gravitational contribution is given by

$$\Delta P_g = \rho_f \frac{g}{g_c} L \sin \theta \, r_g \tag{27}$$

Comparison of the Thom model and the homogeneous model for a steam water system shows that at low qualities, $x < 0.1$, the homogeneous model is good, but at qualities greater than 0.1, the Thom model is superior. Since such a small fraction of the flow system will be at a quality less than 0.1, either the Martinelli method or the Thom method should be appropriate for use. In the Martinelli method the factor C is unknown for a particular system and as a function of gravity, while in the Thom method the gravitational dependence of the multiplier r_f must be obtained, in addition to taking into account the fact that the Thom method is based upon water-steam systems, whereas the present system is a freon system.

It is of interest to observe the functional dependencies in the pressure drop of a two-phase system, as in reference 11. As given in reference 11,

$$\frac{P_{L/L_e}}{P_e} = f\left(M_o, \gamma, Re_v, \frac{\mu_\ell}{\mu_v}, \frac{\rho_v}{\rho_\ell}, \frac{L_o}{D}, Fr\right) \tag{28}$$

where $$Fr = \frac{\rho_v V_v^2}{g \sin \theta \, \rho_\ell D} = \text{Froude Number}$$.

The Froude number represents the ratio of inertial forces to gravitational forces. If the condenser pressure drop is now broken into two portions--a contribution due to gravity effects and the second consisting of all other terms--the Froude number may be

evaluated for two cases of interest. The first case is that in which the gravity contribution to the pressure drop is of second order compared with other losses, for which the following expression should be satisfied:

$$Fr_o \geq 130\ \gamma \left(\frac{\rho_v}{\rho_\ell}\right)^{2/3} M_o^2\ \frac{(L_o)}{D} \tag{29}$$

For the second case, where the gravity contribution to pressure drop is of the same order of magnitude as the other losses,

$$Fr_o \leq 23\ \gamma \left(\frac{\rho_v}{\rho_\ell}\right)^{2/3} M_o^2\ \frac{(L_o)}{D} \tag{30}$$

The expressions (29) and (30) are based upon the following assumptions and conditions:

1. The total condenser pressure drop is 10 percent of the inlet pressure.

2. Static pressure drop at the condenser inlet due to velocity change and inlet and exit losses are not included in other (non-gravity) pressure drop terms.

3. The major portion of the condenser pressure drop occurs in the first 80 percent of the condensing length.

4. Density ratios from 0.05 to 0.0001 are considered.

A detailed development of the criteria presented here may be found in reference 11.

From a practical view, equation (28) states only that there is a functional dependence of pressure drop on Froude numbers, but the particular nature of the dependency is unspecified. Criterion (29) merely states that for large Froude numbers the gravitational contribution to pressure drop is of second order. If, then, one is interested only in order of magnitude differences, it is evident by the definition of the Froude number that for either a zero gravity

condition, or a horizontal system tested in a 1-g environment ($\sin\theta = 0$), the Froude number is infinite, and in both instances the gravitational contribution to pressure drop is negligible. This is consistent with earlier comments herein.

Heat Transfer

The Carpenter-Colburn correlation (ref. 14) was considered the best available for predicting heat transfer during film condensation inside tubes in the analysis of reference 11. The mean heat transfer coefficient for such a case may be written in the form:

$$Nu = \frac{0.065}{\sqrt{2}} Pr_\ell^{1/2} F_2'^{1/2} Re_v \frac{(\mu_v)}{(\mu_\ell)} \left(\frac{\rho_\ell}{\rho_v}\right)^{1/2} \tag{31}$$

where $$Nu = \frac{h_m D}{k_\ell}$$

$$Re_v = \frac{G_t D}{\mu_v}$$

$$F_2' = \frac{F_1}{G_T^2/(2\rho_v)} = \frac{D}{2L\gamma M_o} \frac{\Delta P_T}{P_e}$$

The dimensionless shear stress, F_2, results from friction, gravity and momentum. Since the latter quantities are related to pressure drop, it should be expected that all the dimensionless parameters affecting the pressure drop also affect the heat transfer coefficient. In addition, however, a parameter that is associated with all analyses of condensation heat transfer systems is $C_{p\ell}(T_s - T_w)/(h_{\ell v} Pr_\ell)$. Thus the functional dependence of the condensing heat transfer coefficient may be expressed in the form:

$$Nu = f\left(Pr_\ell, \frac{C_{p\ell}(T_s - T_w)}{Pr_\ell h_{\ell v}}, M_o, \gamma, Re_v, \frac{\rho_\ell}{\rho_v}, \frac{L_o}{D}, \frac{L}{L_o} Fr\right) \tag{32}$$

As in the case of pressure drop, the magnitude of the Froude number should indicate the magnitude of the gravitational effect upon heat transfer. In fact, the criteria expressed by (29) and (30) should also be applicable for heat transfer. Specifically, according to reference 11, for large Froude numbers (low gravity fields), the condensation heat transfer coefficient should be affected less than 5 percent by gravity effects. For small Froude numbers, the gravity, friction, and momentum upon heat transfer are of the same order of magnitude. However, in a zero-g environment, or in a horizontal system in a 1-g field, the Froude number will be infinite.

Some insight into possible zero-g effects on heat transfer may be obtained by examining the annular flow model. The annular flow regime is of importance since it can exist over a large fraction of the flow system length. Annular flow generally occurs when the void fraction is greater than 80 percent. Examination of the Martinelli-Nelson plot of void fraction versus quality for a steam-water system over a range of system pressures indicates that at pressures of 200 psia, annular flow should be expected to occur over 85 percent of the flow channel length, using the preceding rule of thumb and assuming a linear quality variation along the channel length. (In the present condensing system annular flow was observed over roughly 75 percent of the channel length.)

In annular flow the gas and liquid velocities are generally not the same. Waves are formed at the interface, consequently, giving rise to form drag on the waves, which is reflected in the increased pressure drop observed for annular flows. Such interfacial action affects the magnitude of the interfacial friction factor, C_{fi}, which when taken with the wall friction coefficient, C_{fw}, permits evaluation of the pressure drop and void fraction (Ch. 11, ref. 15). Heat transfer characteristics are also related to these friction coefficients, and in this respect it is significant that a marked, substantial decrease in C_{fi} occurs when the annular flow is "smooth," rather than "rough" (fig. 2, also fig. 3.6, ref. 9). It is of significance since a smooth(er) interface would be expected under 0-g conditions.

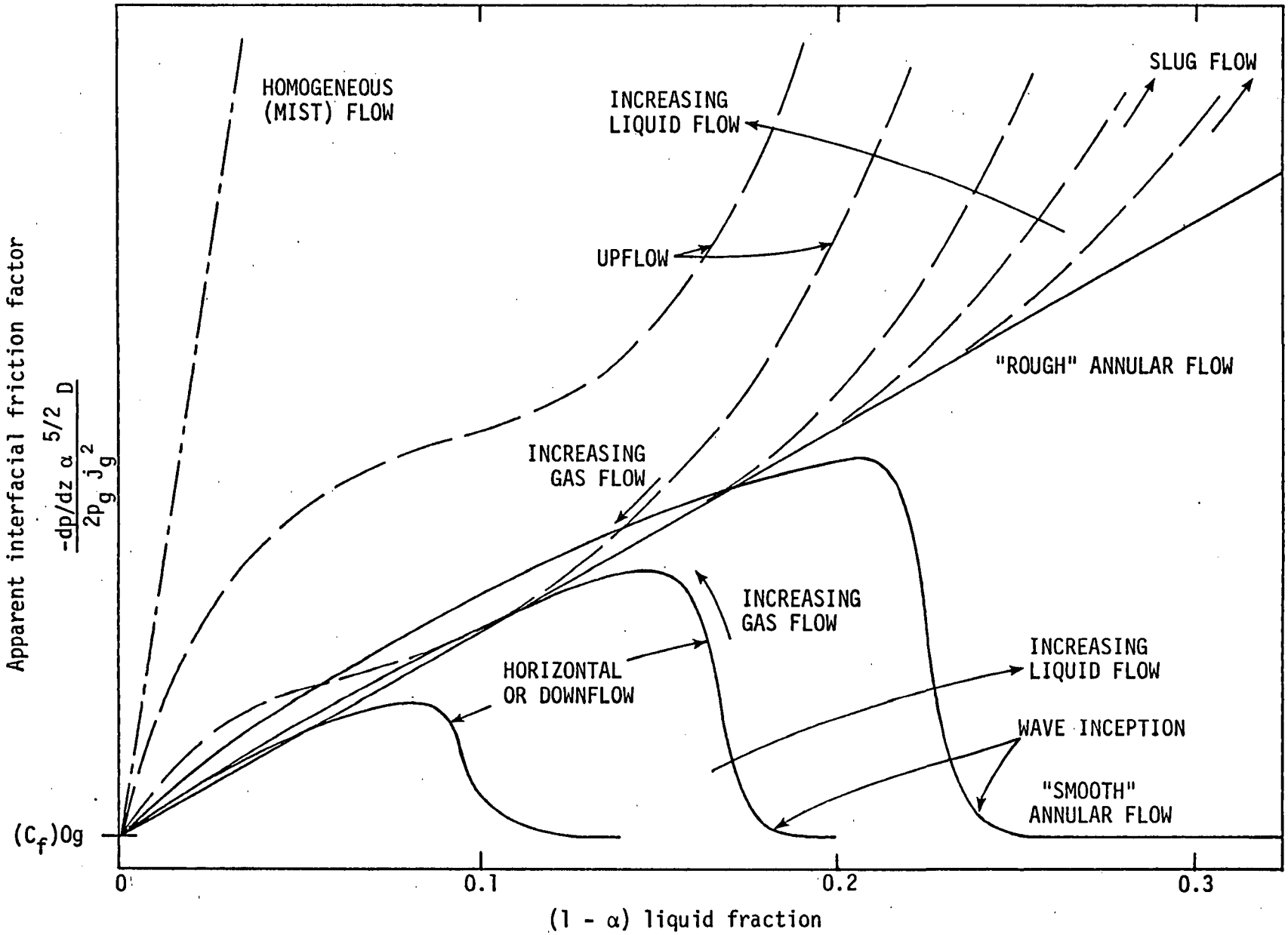

Figure 2. Pressure drop characteristics of different flow regimes in terms of apparent interfacial friction factor.

Perhaps the best heat transfer analysis of flow condensation systems is that of Bae, Maulbetach, and Rohsenow (ref. 16). Their analysis is approximate in that it is based on the assumption of annular flow throughout the flow channel. It is perhaps the most practical, however, and for many flow situations the assumption of totally annular flow is not unrealistic (discussed earlier).

Their results for the heat transfer coefficient are as follows:

$$Nu_z \equiv \frac{h_z D}{k_\ell} = \frac{\rho_\ell c_\ell D\, u_\tau}{k_\ell F_2} \tag{33}$$

or

$$St_z^* \equiv \frac{h_z}{\rho_\ell c_\ell u_\tau} = \frac{1}{F_2} \tag{34}$$

where $$u_\tau = \sqrt{\frac{g_o \tau_o}{\rho_\ell}} \tag{35}$$

and

$$\text{for } 0 < \delta^+ < 5: \quad F_2 = \delta^+ \, Pr \tag{36a}$$

$$\text{for } 5 < \delta^+ < 30: \quad F_2 = 5Pr + 5\ell n \left[1 + Pr\left(\frac{\delta^+}{5} + 1\right)\right] \tag{36b}$$

$$\text{for } \delta^+ > 30: \quad F_2 = 5Pr + 5\ell n\,(1 + 5Pr) + \frac{2.5}{\sqrt{1 + \frac{10}{Pr}\frac{M}{\delta^+}}}\, x$$

$$x\ell n \left[\frac{2M - 1 + \sqrt{1 + \frac{10}{Pr}\frac{M}{\delta^+}}}{2M - 1 - \sqrt{1 + \frac{10}{Pr}\frac{M}{\delta^+}}} \cdot \frac{\frac{60}{\delta^+} M - 1 - \sqrt{1 + \frac{10}{Pr}\frac{M}{\delta^+}}}{\frac{60}{\delta^+} M - 1 + \sqrt{1 + \frac{10}{Pr}\frac{M}{\delta^+}}}\right] \tag{36c}$$

Here

$$M \equiv \frac{F_o \, \delta^+ \, \nu_\ell}{\tau_o \, u_\tau} \tag{37}$$

and

$$\delta^+ \equiv \delta \, u_\tau / \nu_\ell \tag{38}$$

Further, Re_ℓ is defined as

$$Re_\ell = \frac{(1 - x)GD}{\mu_\ell} = \frac{4\Gamma}{\mu_\ell} = \frac{4}{\mu_\ell} \int_o^\delta \rho_\ell v_z dy = 4 \int_o^{\delta^+} v_z^+ dy^+ \tag{39}$$

and is evaluated from the following velocity distribution assumed in the liquid layer:

$$\begin{aligned} 0 < \delta^+ < 5 \qquad & v_z^+ = y^+ \\ 5 < \delta^+ < 30 \qquad & v_z^+ = -3.05 + 5 \ln y^+ \\ 30 < y^+ \qquad & v_z^+ = 5.5 + 2.5 \ln y^+ \end{aligned} \tag{40}$$

where

$$v_z^+ = v_z / \sqrt{g_o \tau_o / \rho} = v_z / u_\tau ; \qquad \delta^+ = \frac{\delta}{\nu} \sqrt{\frac{g_o \tau_o}{\rho}}$$

with the following results:

$$\delta^+ < 5 \qquad Re_\ell = 2(\delta^+)^2 \tag{41a}$$

$$5 < \delta^+ < 30 \qquad Re_\ell = 50 - 32.2 \, \delta^+ + 20. \, \delta^+ \ln \delta^+ \tag{41b}$$

$$\delta^+ > 30 \qquad Re_\ell = -256 + 12 \, \delta^+ + 10 \, \delta^+ \ln \delta^+ \tag{41c}$$

For any assumed magnitude of Pr, δ^+ and M, one can calculate Re_ℓ from equation (41), F_2 from equation (36) and St^* from equation (34). Then curves of St^* vs. Re_ℓ for various M can be constructed.

The calculation procedure starts by dividing the tube length in increments of changes in quality x. For a given flow rate and fluid conditions one then calculates the increment of length required to accomplish this quality change. The calculation is a step-wise one requiring trial-and-error at each step. Further details of the procedure and the development of the preceding equations may be found in reference 16.

For the case of uniform wall temperature, such as would exist in the condensing portion of the channel, a mean heat transfer coefficient, defined by

$$h_m = \frac{1}{L}\int_o^L h_z \, dz \tag{42}$$

is found to be

$$\frac{1}{h_m} = \frac{1}{x_e}\int_{x_e}^1 \frac{dx}{h_z} \tag{43}$$

It is of interest to attempt to estimate the influence of a varying gravitational environment on the heat transfer coefficient that is indicated by equations (33) and (34). It is obvious that such a dependency must be contained in the factor F_2, which takes on three different values in the liquid film, as indicated in equation (36). In the laminar sublayer, it may be seen that F_2 is proportional to $(\sqrt{F_o}\,\delta^{3/2} + \tau_v\,\delta)$, or δ^+, while in the buffer layer, $5 < \delta^+ < 30$, F_2 is proportional to $\ln(\sqrt{F_o}\,\delta^{3/2} + \tau_v\,\delta)$, or $\ln \delta^+$. In the fully turbulent region, $\delta^+ > 30$, the dependence on δ^+ appears to be very weak.

From the preceding proportionalities, in a zero-g environment F_o would be reduced by the quantity $\frac{g}{g_c}\rho_\ell$, since

$$F_o \equiv -\frac{dP}{dz} + \frac{g}{g_c}\rho_\ell - \frac{1}{g_c A_{z_\ell}}\left[\frac{d(u_\ell W_\ell)}{dz} - U_i \frac{dW_\ell}{dz}\right] \qquad (44)$$

but the effect of this reduction is reduced somewhat since $h_z \alpha \sqrt{F_o}$ in the laminar sublayer, and $h_z \alpha \ln \sqrt{F_o}$ in the buffer layer, knowing that

$$\tau_o = F_o\delta + \tau_v. \qquad (45)$$

It is also seen that h_z is proportional to $\delta^{3/2}$ and $\ln \delta^{3/2}$ (and also τ_v). While it is not clear how τ_v might vary with gravity, it is clear from preliminary zero-g test observations that δ will vary with gravity, in the sense that at 1-g conditions liquid tends to gather at the bottom of the channel, while at 0-g conditions the liquid distributes itself uniformly about the channel wall. The effects of this redistribution warrant additional investigation, as it appears that the greatest influence upon the heat transfer coefficient changes in a changing gravitational environment are a result of the liquid film re-distribution about the channel walls.

Instability

Flow instabilities are undesirable for a variety of reasons. Some possible undesirable effects that may arise because of flow instabilities are: (1) forced mechanical vibration of system components, (2) system control difficulties, and (3) decreased heat transfer performance. Generally, then, one must either predict the conditions which will lead to serious instabilities or design the system to compensate for such conditions.

A comprehensive classification, description, and summary of two-phase flow instabilities may be found in reference 11, together

with selected stability analyses of flow condensation systems. Design calculations for the condenser/radiator system studied herein is found in references 1 and 17.

After analyzing the various types of instabilities that might occur in a parallel flow multi-tube condensation system it was concluded in reference 11 that the three types of instability that could significantly affect the condensation system performance (i.e., result in fluctuations of temperature, flow and quality distribution), are (a) gravity induced runback, (b) gravity distortion of the interface, and (c) negative pressure drop gradient.

Gravity induced runback occurs when the shear force in the condensing liquid film goes to zero at the tube wall, i.e., when the gravitational forces are of the same order as the vapor shear forces. However, such a problem will occur only in the presence of an axial gravitational field, and consequently should not exist in a 0-g field. Certainly testing a condenser system in a vertical upflow condition in a 1-g environment should provide the most adverse operating conditions for a system expected to function in a 0-g environment.

In general, the various types of instabilities that may occur are governed by balances among the following forces: inertial, surface tension, viscous, and acceleration. The pertinent dimensionless parameters representing ratios of these forces are: (a) Reynolds number (inertial/viscous forces), (b) Froude number (inertial/gravitational forces), (c) Weber number (inertial/surface tension forces), and (d) Bond number (acceleration/surface tension forces).

The design of the radiator/condenser panel tested here is based upon the criteria that a stable annular flow will exist for either the liquid film Reynolds number (Re_δ) being less than 200, or the Weber number being less than 3 for any value of Re_δ (ref. 18). Certainly annular flow does not persist for the entire region of the condensing flow, but the portion in annular flow constitutes the major portion of the flow channel, as observed in ground tests of the transparent radiator/condenser panel model. The analyses

of reference 11 similarly indicate that for a flow that is largely annular, other types of hydrodynamic instabilities, such as that associated with the transition from annular to slug flow, are not significantly large.

Additionally, the problem of gravity distortion of the interface may be avoided if the channel diameter is smaller than the maximum stable critical diameter (ref. 19),

$$D_c = 1.835 \left[\frac{\sigma}{(\rho_f - \rho_g) \frac{g}{g_c}} \right]^{1/2} \tag{46}$$

as is the case with the present r/c system.

Finally, the system instability associated with a negative system pressure drop gradient (Ledinegg, ref. 20), is conceivable only if the momentum pressure recovery of the vapor phase is greater than the frictional pressure drop (and gravity drop if operated vertically upward). Early results of ground tests of the system indicate no such instabilities, or pressure rises.

A further elaboration and discussion of instability phenomena and criteria are presented in Appendix A.

EXPERIMENTAL DESCRIPTION

The principal item tested here was a full-scale radiator/condenser panel that consisted of nine parallel connected flow channels (2.41 mm dia, and 3.66 m length) on 22.86 cm centers, welded to a flat aluminum panel, as illustrated in figure 3 (panel no. 1). The r/c panel was designed to accomplish the following (ref. 21):

1. Have the same external dimensions as the individual shuttle orbiter radiator panels (6-ft [1.83 m] wide by 12-ft [3.66 m] in length).

2. Operate at a maximum condensing temperature of 150 deg F (338.9 deg K).

3. Reject up to 9000 BTU/hr (2.637 kW) to a sink temperature of 0 deg F (273.15 deg K).

4. Use constant area parallel flow passages of about 1/8 in. (3.18 mm) i.d.

5. Have a flowrate of at least 40 lb/hr-tube (5.04 g/s-tube) in the all-liquid operating mode (sufficient to provide turbulent flow).

6. Incur a maximum r/c pressure drop of 5 psi (35 kPa) in the all-liquid mode and 4 psi (28 kPa) in the vapor-cycle mode.

7. Maintain hydrodynamically stable flow in the r/c in the vapor-cycle mode, such that no vapor is introduced into the r/c outlet manifold.

8. Provide positive liquid collection at the outlet header.

9. Operate successfully with an acceleration of 0.1-g along any axis of the radiator.

It was necessary to test the panel under 1-g conditions in order to verify the preceding operational goals, particularly with regard to heat transfer, pressure drop, and stability. However, testing in a 0-g environment was also believed essential in order to determine whether the operating characteristics changed significantly from those under a 1-g force field. As indicated previously, however, no useful zero-g data was obtained.

In order to obtain some insight into the two-phase flow and heat transfer behavior of the full-scale r/c system, a second system of three parallel-connected transparent quartz tubes, modelled thermally and hydraulically after the full-scale panel, was fabricated to permit high-speed photography of the two-phase flow phenomena. The systems are shown in figures 3 to 5.

The test apparatus schematic for the two systems is shown in figure 5. The condensing fluid refrigerant-12 (R-12), is stored in a 75.7 liter tank that can be heated to provide the desired system operating pressure (0.0984 to 0.246 kgf/mm^2) by an immersion-type heater. The liquid R-12 withdrawn from the tank bottom passes

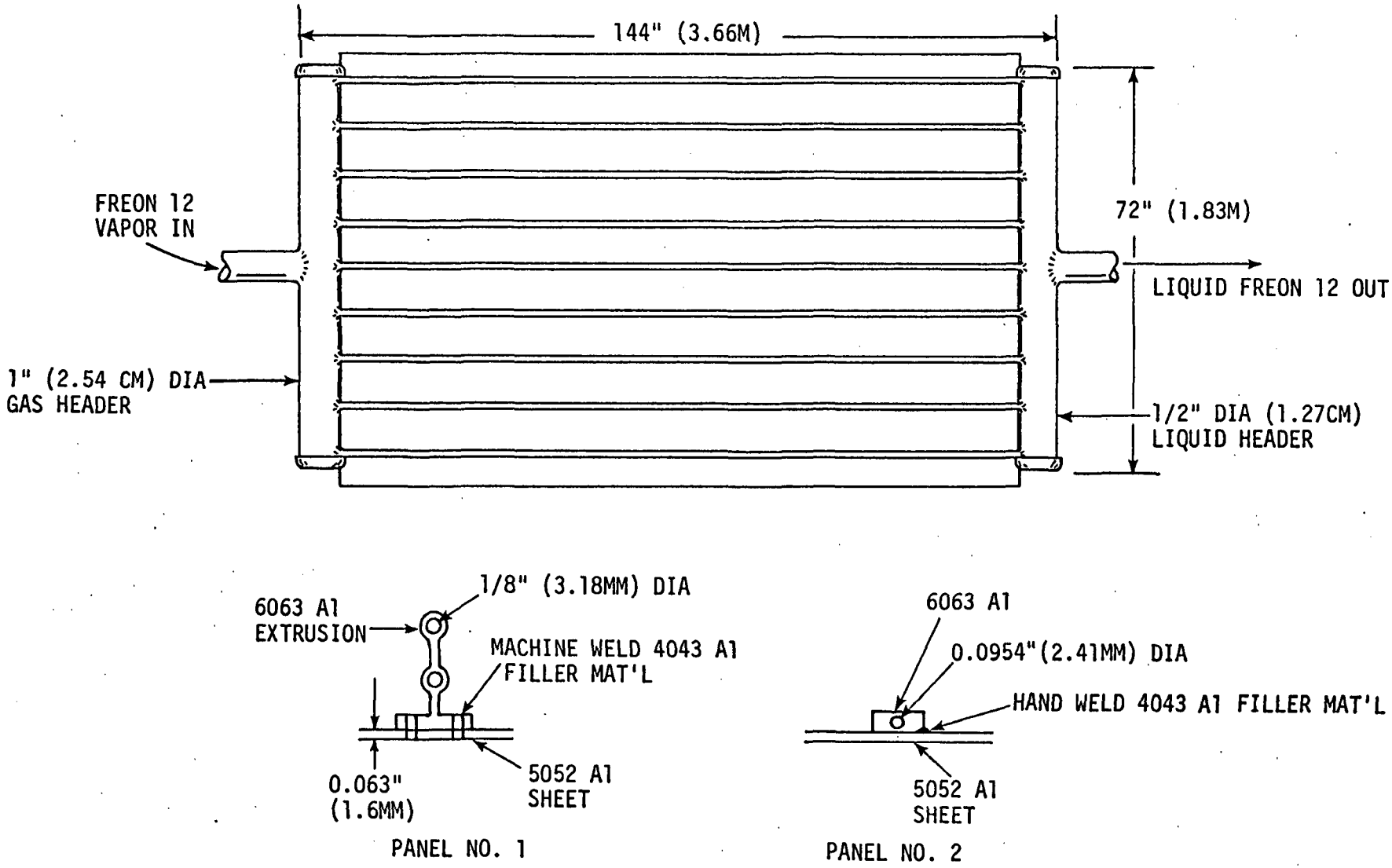

Figure 3. Radiator/condenser panel design.

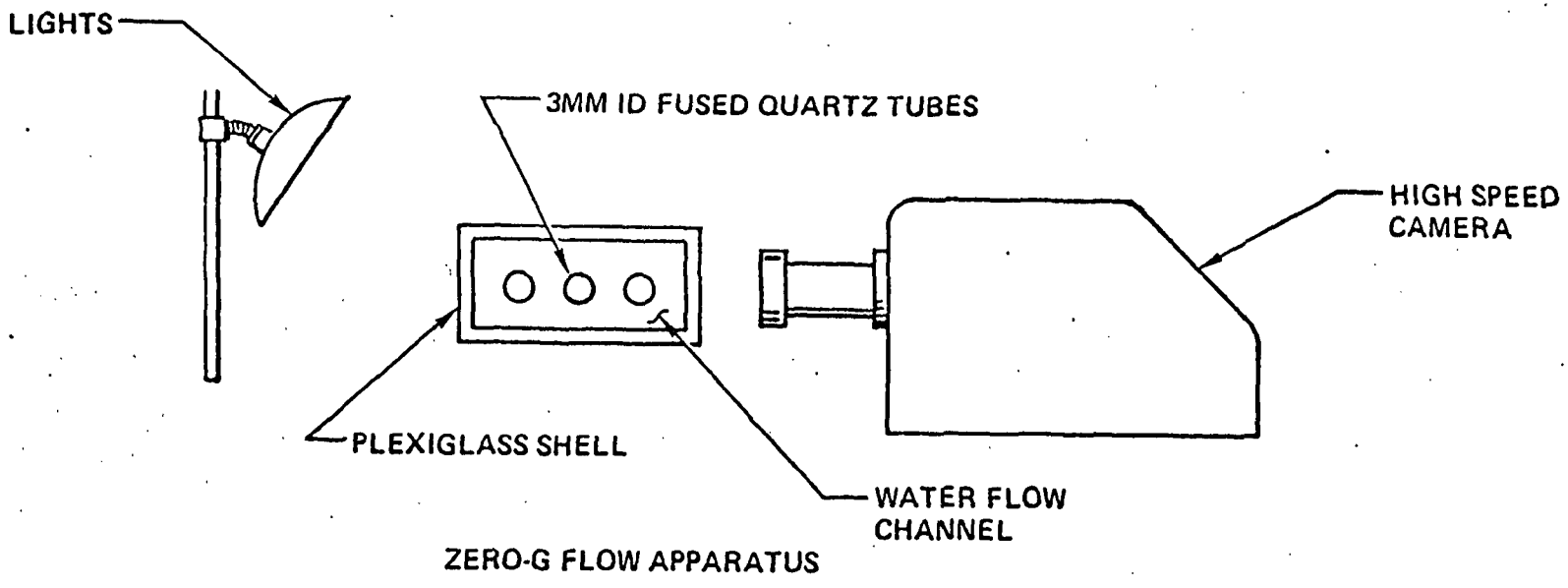

Figure 4. Flow visualization apparatus.

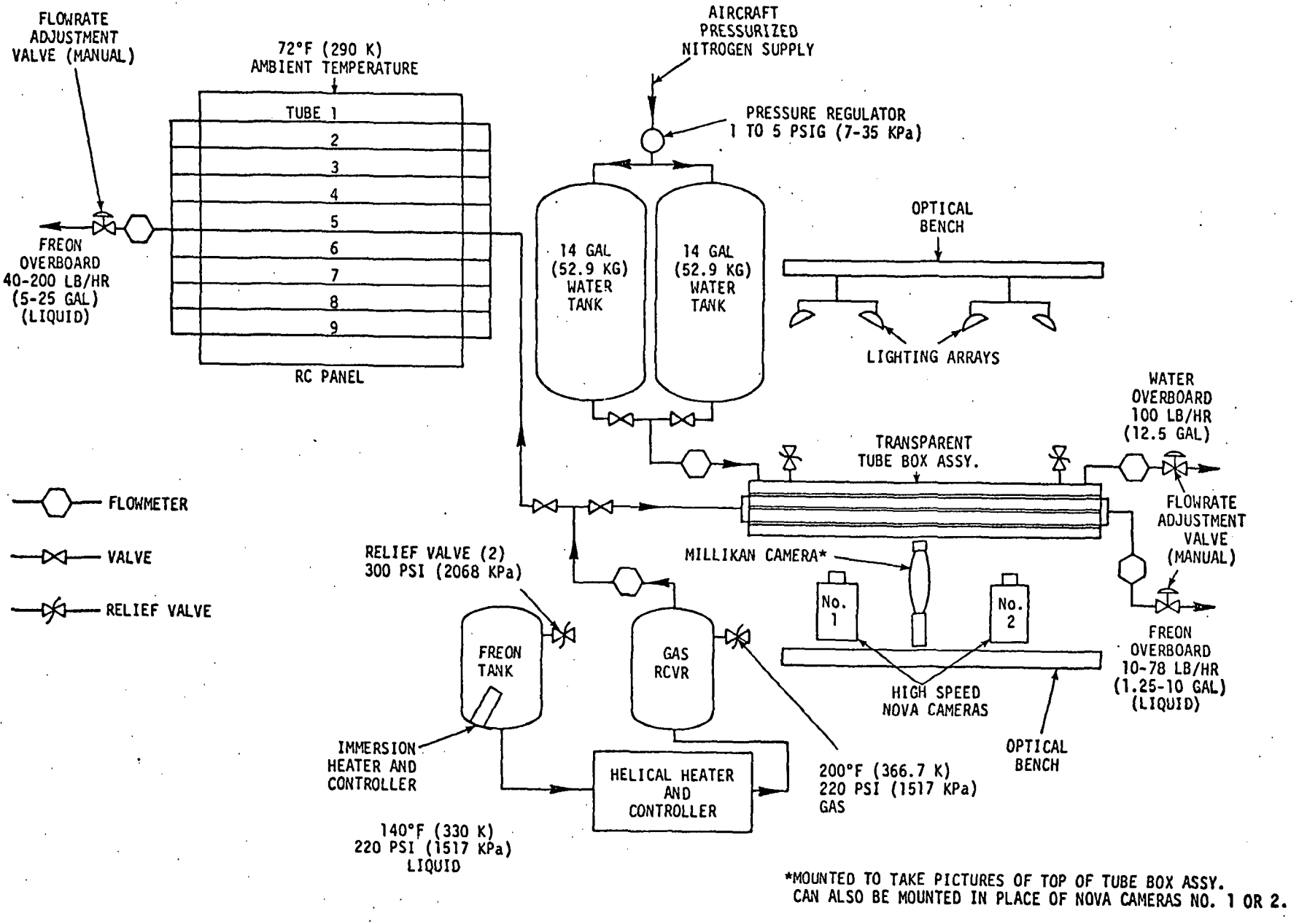

Figure 5. Test apparatus flow schematic.

through an electrical heating system where the R-12 is superheated to the desired degree. The heater is designed with a tortuous pathway system so that centrifugal forces maintain the liquid refrigerant in contact with the heater walls during weightless intervals. The R-12 then flows to a gas receiver so that any pressure fluctuations caused by flashing in the boiler may be damped out.

The superheated R-12 vapor flow is then directed to either the r/c panel or to the transparent tube fixture. In either case the exiting liquid R-12 passes through a flow metering valve which maintains the flowrate at the desired level 2.3 to 9.1 kgm/hr. The condensed R-12 is then either dumped overboard or to the atmosphere, depending upon whether flight tests (0-g) or ground tests are being conducted.

The quartz tube fixture is cooled by water (figs. 4, 5) stored in two 53-liter tanks in a closed loop parallel flow system (though in some initial tests an open coolant system was employed). The water temperature in the tanks ranged from 15.6° to 26.7°C, while the nominal flowrate was 45.4 kgm(m)/hr. The maximum temperature rise of the water was 17°C. The inlet R-12 temperature ranged from 47.2° to 86.7°C while pressures ranged from 0.110 to 0.179 kgf/mm^2. The quartz tubes are nominally 3 mm i.d. and 8 ft (2.44 m) long.

Instrumentation on the transparent tube fixture consisted of inlet and outlet temperatures (immersion thermocouples) and pressures of the R-12, together with ΔP measurements across the quartz tube assembly. The inlet and exit temperature of the water system were also monitored by immersion thermocouples. Four surface temperature measurements of the plexiglas flow channel were also made. Flowrate measurements of both systems were made with turbine flow meters, while a rotameter was employed in the water system for 1-g tests.

The total number of measurements taken were: 4 flow rates, 9 absolute pressures, 7 differential pressures, 3 components of acceleration, 55 temperatures, 2 camera event markers, and 1 thermocouple reference junction temperature (see fig. 6). The data

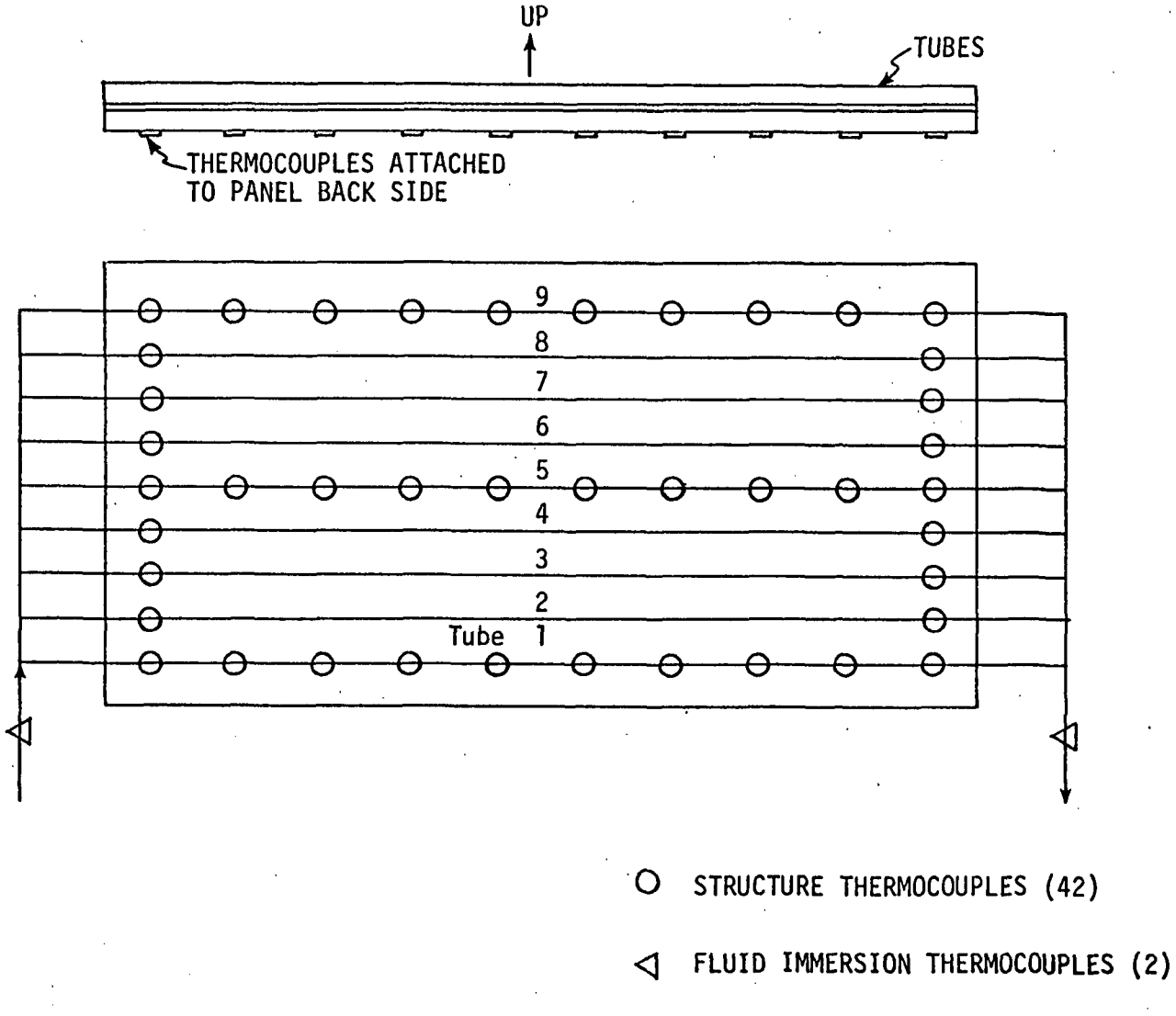

Figure 6. Instrumentation schematic of r/c panel.

acquisition system employed digital and analog systems, in addition to visual monitoring of the overall experimental system. The digital system employed was a Wright-Patterson AFB binary code digital recording system that is described in detail in references 22 and 23. The oscillographic recorder was a Honeywell Model 1108 that recorded 23 channels of data.

The photographic observations were made with two high speed cameras (operated at 2000 to 7000 frames/second) and a low speed camera (400 frames/second). The low speed camera was mounted so as to view all three tubes from above, permitting observation phenomena within the parallel system. All three cameras were mounted on optical benches that permitted rapid repositioning along the length of the tubes. The high speed cameras viewed the transparent fixture from the side, as shown in figures 4 and 5.

The experimental equipment was modified somewhat after initial zero-g testing had dictated the desirability of certain system design and instrumentation changes (ref. 22). Since no zero-g data is presented herein, however, such changes are irrelevant to this report.

Measurements were obtained from the high speed photographs of film thickness, wavelength (distance between growing disturbances on the liquid film), and liquid and vapor velocities. Vapor bubble velocities were easily obtained in the low quality regions, but elsewhere both liquid and vapor velocities were difficult to measure directly.

Measurements were made using a Vanguard Motion Analyzer. In obtaining such measurements of flow characteristics within the small diameter tube, it was first necessary to determine whether the curvature of the tube walls distorted appreciably the physical dimensions of the phenomena being observed. This was accomplished by inserting a finely graduated (0.02 in.) scale into the end of a section of such tubing and comparing the graduations appearing both inside and outside the tubing. No distortion was observed across the entire tube diameter.

EXPERIMENTAL RESULTS

Flow Regimes

It is of practical interest to obtain knowledge of the flow regimes in a given two-phase system for several reasons. The primary reason is that both heat transfer and pressure drop characteristics are related to the particular flow patterns existing in a system, and the range (channel length) over which each of these patterns occurs. Such a picture of the types of flow regimes existing and their boundaries is useful in indicating the reasonableness or limits on the validity of a particular analytical model. Finally, in the present study a comparison of the 1-g and 0-g flow patterns could provide insight in understanding and predicting 0-g behavior (heat transfer and pressure drop), and ultimately lead to modifications of design procedures normally applicable only to 1-g conditions.

In the present study only 1-g photographs were available for examination. The flow regimes and transitions characterizing the system are shown schematically in figure 7. This figure has been developed after examination of numerous high-speed photographs taken at different locations along the condenser tube's length. The actual tube diameter in this case was 2.62 mm. Flow rates of the condensing R-12 ranged from 2.3 to 9.1 kg/hr, corresponding to G values of 42.2 to 168.9 x 10^4 kg/m^2-hr. Inlet temperatures varied from several degrees superheat to saturation temperature. Over this range of flow variables no substantial differences were observed in this qualitative, schematic illustration of flow patterns shown in figure 7. Actual photographs of the flow patterns may be found in reference 2.

The flow regimes observed are compared with those predicted by the Baker chart (ref. 24) in figure 8. The coordinates of figure 8 are functions of liquid and vapor mass flowrate and fluid properties (viscosity, surface tension, density). The flow regimes observed herein were categorized into four groups: annular, annular-stratified, slug, and bubbly (ranges from long elongated

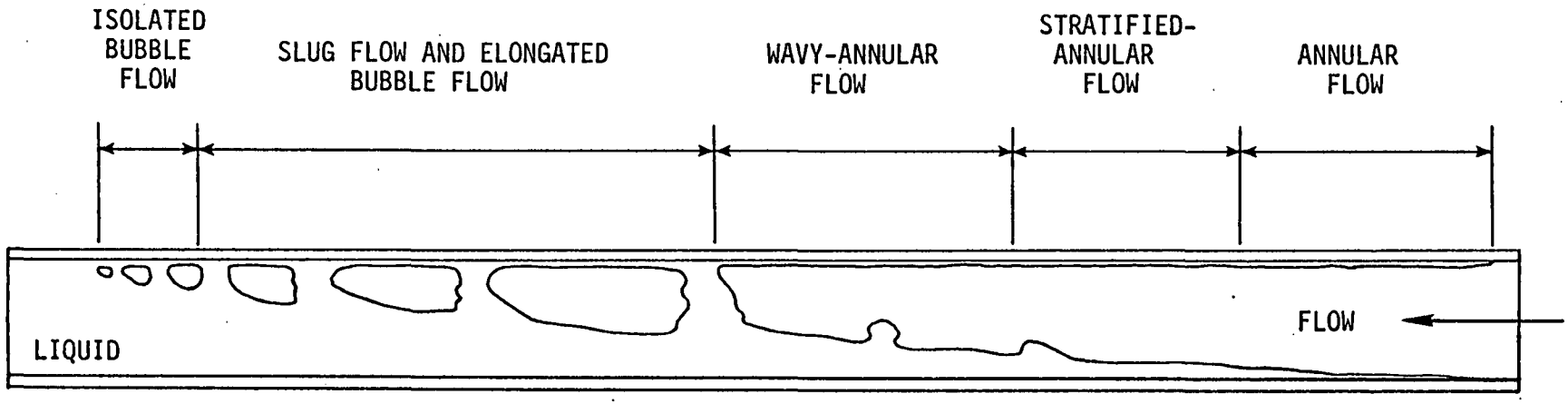

Figure 7. Schematic of characteristic flow regimes.

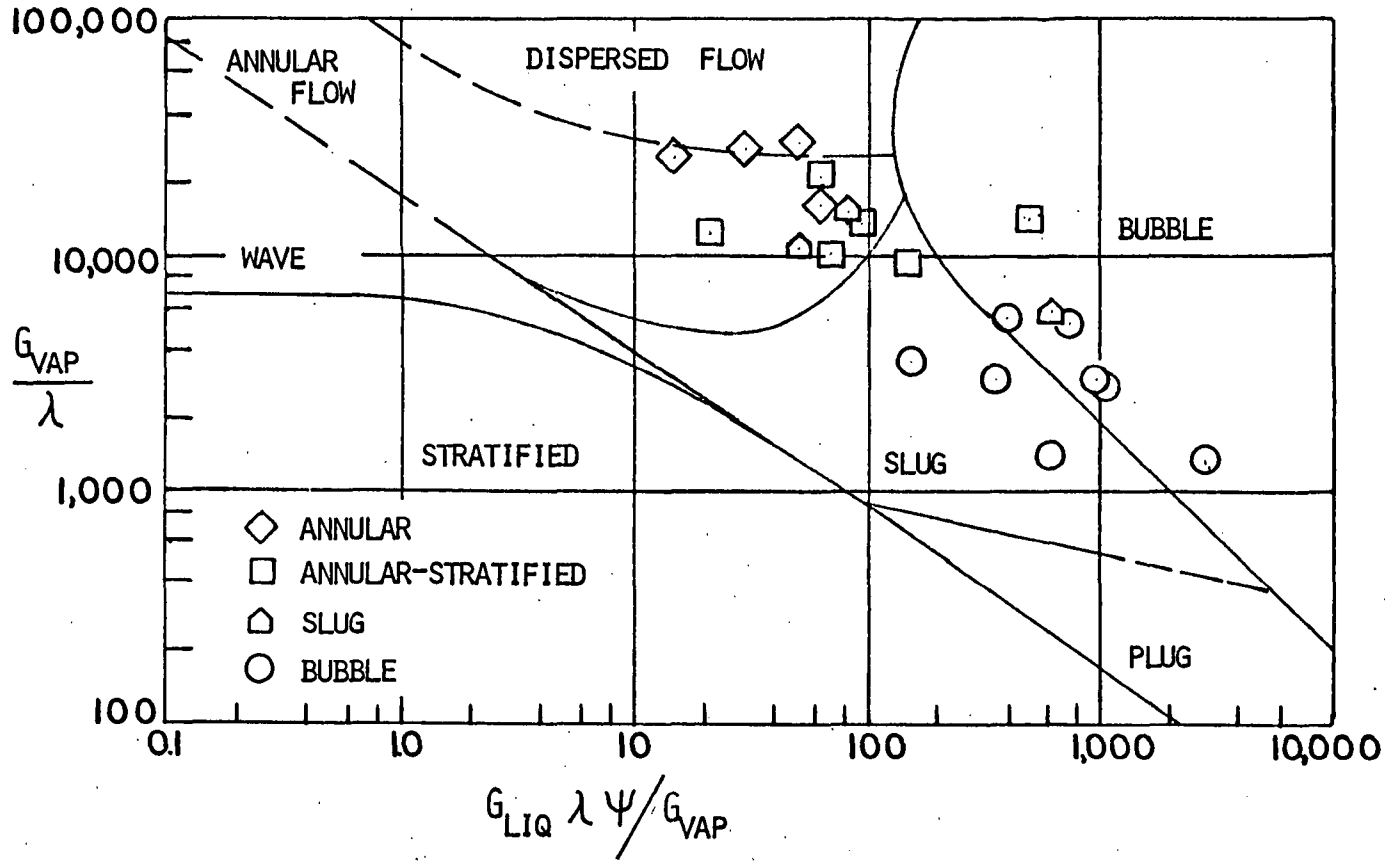

Figure 8. Baker chart.

bubbles to small isolated bubbles traveling at the top of the tube). The number of flow regimes into which the flow was divided was chosen as the minimum number consistent with describing fundamentally differing flow regimes. Additional subdivision did not appear to be very meaningful, since two, or even three, flow patterns were not infrequently observed to exist at the same viewing location within a period of less than one second (see photographs in ref. 2). Furthermore, this variety of flow patterns at a single location occurred in a basically steady flow, i.e., the point of complete vapor extinguishment did not oscillate noticeably.

Regarding the stratified-annular regime, a few comments are in order regarding semantics. This regime seems to correspond with the semi-annular flow of reference 31, excepting that no liquid film covered the top of the inside tube wall in the semi-annular flow. The terminology of "wavy flow" is sometimes employed in the literature as representing the transition region between annular and slug flow. The wavy region, per se, was not treated herein as a separate flow regime, but rather only as part of the stratified-annular regime. The stratified-annular regime herein included flows where the liquid layer was at times relatively smooth and undistorted, at times wavy, and at times sufficiently wavy to permit bridging of the tube diameter by the wave tops. In all cases, a thickness of liquid was present around the entire tube periphery, though the liquid film buildup occurred only along the tube bottom due to gravity-induced drainage from the upper portions of the tube wall.

In order to determine the length of the flow channel occupied by different flow regimes, all of the flow regime data for the various test runs were plotted in figure 9 as a function of quality, without regard to system pressure or mass flow rates. In this plot an additional flow regime is included, namely the stratified-annular region where frequent bridging occurs (i.e., the wave tops completely reach across the tube diameter). As indicated earlier, distinguishing this flow regime was not judged necessary, and this is partially because of the results of figure 9.

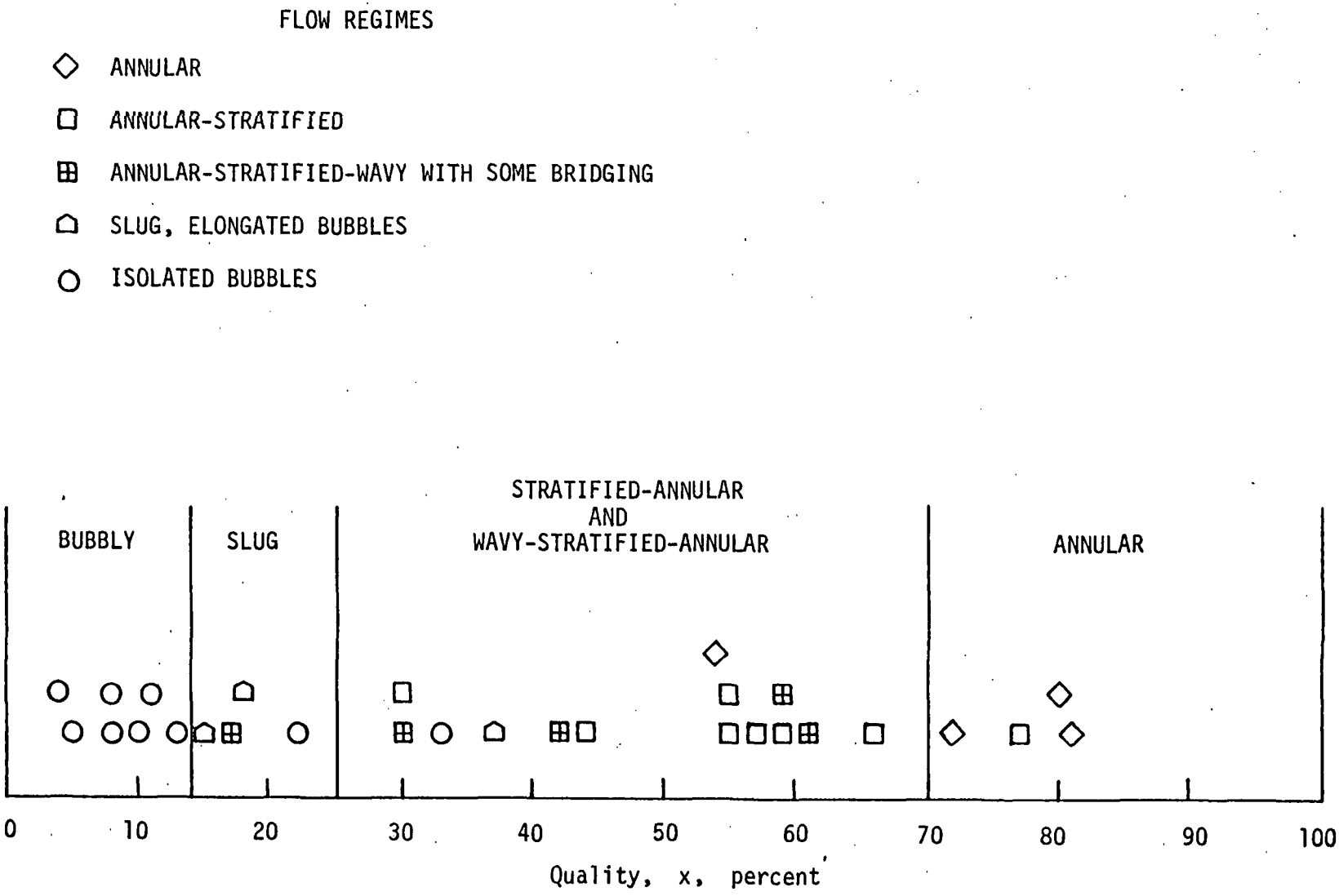

Figure 9. Flow regime distribution with quality, as determined from photographic observations.

As seen, there are certainly not sharp boundaries indicated by the plotted data, as is to be expected with two-phase flows. Nevertheless, it does seem apparent that dividing the tube into separate flow regime portions as in figure 9, on the basis of the flow regime observations plotted, is quite reasonable. It is apparent that the central portion contains at least one data point for each flow regime, though it obviously contains a preponderance of annular-stratified-bridged data points. Since the bridged-stratified and the simple stratified-annular regimes are quite interspersed, and since photographic results presented earlier (ref. 2) indicate that three regimes were observed at the same channel location within a 1-second period of the flow, it does appear reasonable that further distinction between these two regimes is not necessary.

It is of importance to observe that a rather large fraction of the flow, about 75 percent, is in the annular or annular-stratified regimes. This is of significance since the heat transfer analysis of condensation systems by Bae (ref. 16), discussed earlier, and the modified heat transfer model presented herein are based upon the existence of annular flow over the complete condensing length.

It is also important to note that some 0-g films were obtained, which, while not of sufficiently good quality to obtain quantitative measurements from, were capable of providing a qualitative comparison of 1-g and 0-g flow patterns. It was observed that in the annular flow region, the liquid film was evenly distributed about the inside tube wall, and was noticeably less irregular and wavy. Also, in a 1-g environment, high-velocity disturbances (vapor flow) appeared to disrupt the liquid film appreciably at regular intervals. Under 0-g conditions the periodic high-velocity disturbances did not disappear, but appeared to disrupt or distort the annular film to a much smaller degree. Also, in the bubble flow region, the bubbles moved very nearly along the tube center, showing no affinity for the tube wall.

Measured Flow Characteristics in Annular Flow

Film thickness, quality and void fraction.- Experimental measurements of the liquid film thickness (at the quartz tube bottom) in the annular flow region are tabulated in table 1. The values of quality are those presented in reference 3. The range of reduced pressures (P/P_{crit}) for these measurements ranged from about 0.26 to 0.40. The film thickness was measured from the high-speed motion picture photographs using a Vanguard Motion Analyzer. The scale factor employed was the inside diameter of the tube itself, which was 0.103 inches.

A simplified model of annular flow in a circular tube, assuming a uniform film thickness about the inner wall, relates void fraction, α, and film thickness, δ, by

$$\alpha = 1 - 4\frac{\delta}{D} + 4\left(\frac{\delta}{D}\right)^2 \tag{47}$$

In turn, the void fraction may be related to the quality, x, by the Zivi equation (see figs. 10 and 11),

$$\alpha = \frac{1}{1 + \left(\frac{1 - x}{x}\right)\left(\frac{\rho_v}{\rho_\ell}\right)^{2/3}} \tag{48}$$

which has been found to agree quite well with experimental measurements. Alternatively, one may use the void fraction-quality relationship of Martinelli and Nelson shown in reference 9, p. 43, for steam-water mixtures. Using this figure for other fluids would necessitate comparison of the fluid systems on a reduced pressure basis.

The film thickness measurements are compared here by first calculating the void fraction from equation (47), and then calculating α from Zivi's equation, considered as the standard here using the quality values supplied in reference 3. The value of δ measured at the bottom of the tube was modified, however, since

Table 1. Measurements of film thickness, liquid-, vapor-, and bubble-velocity, and disturbance wavelengths, obtained from high-speed motion picture photographs.

Test No.-Run No.	$G \times 10^{-5}$ lbm/hr-ft^2	$P_{in.}$ lbf/in.^{2}	T_{sat} °F	x %	Flow Regime*	δ in.	V_v in./sec	V_ℓ in./sec	V_b in./sec	λ in.
4-1	1.037	165	117	30	⊞				9.59	
4-2	1.555	169	119	8	○					
4-2	1.555	169	119	77	□	.0202	30.0			.1798
4-3	1.555	172	120	18	⌂				8.74	
4-3	1.555	172	120	-	◇	.0264	32.9			.151
4-4	1.555	170	119	59	⊞	.0247				
4-5	1.555	176	122	59	□	.031	20.8			.168
4-6	2.535	162	115	15	⌂				14.9	
4-6	2.535	162	115	81	◇					
4-6	2.535	162	115	41	○				1.91	
4-7	2.506	157	113	30	□	.031				.181
4-7	2.506	157	113	54	◇	.020				.081
4-8	3.456	219	139	13	○					
4-8	3.456	219	139	42	⊞	.0297				.118
4-9	3.255	218	139	4	○					
4-9	3.255	218	139	80	◇	.0187				
3-1	3.255	232	144	4	○					
3-1	3.255	232	144	44	□	.0072	33.6			.184
3-2	3.226	232	144	66	□	.016				.149
3-3	3.168	232	144	17	⊞				4.03	

* See figure 9 for key to symbols.

(cont'd.)

Table 1. Measurements of film thickness, liquid-, vapor-, and bubble-velocity, and disturbance wavelengths, obtained from high-speed motion picture photographs (concluded).

Test No.-Run No.	G x 10^{-5} lbm/hr-ft^2	$P_{in.}$ lbf/in.^{2}	T_{sat} °F	x %	Flow Regime*	δ in.	V_v in./sec	V_ℓ in./sec	V_b** in./sec	λ in.
3-3	3.168	232	144	37	⌂	.026	28.0			
3-4	2.678	232	144	–	○				(T)5.81 (M)9.36	
3-5	2.708	232(?)	147	10	○				13.0	
3-6	2.765	238	146	55	□	.0401	29.5	20.1		.168
3-6	2.765	231	144	55	□					
3-7	1.872	231	144	~8	○				7.15	
3-8	1.381	231	144	~22	○				(T)3.07 (M)3.54 (B)2.21	
3-9	1.383	231	144	33	○				10.1	
3-10	3.917	233	145	72	◇	.0122				
3-10	3.744	233	145	72	◇	.0122				
3-11	2.592	231	144	11	○				9.2	
3-11	2.592	231	144	61	⊞	.0232				.133
3-12	2.621	231	144	57	□	.0209				.114
5-1-10	3.456	255		~50						.1065
5-1-10	3.456	255		~50		.0288				.134
5-1-12	3.456	255		~40		.0200				
5-1-13	3.456	255		~5					5.12	

* See figure 9 for key to symbols.
** (T), (M), (B) = Top, Middle, or Bottom tube as viewed by camera.

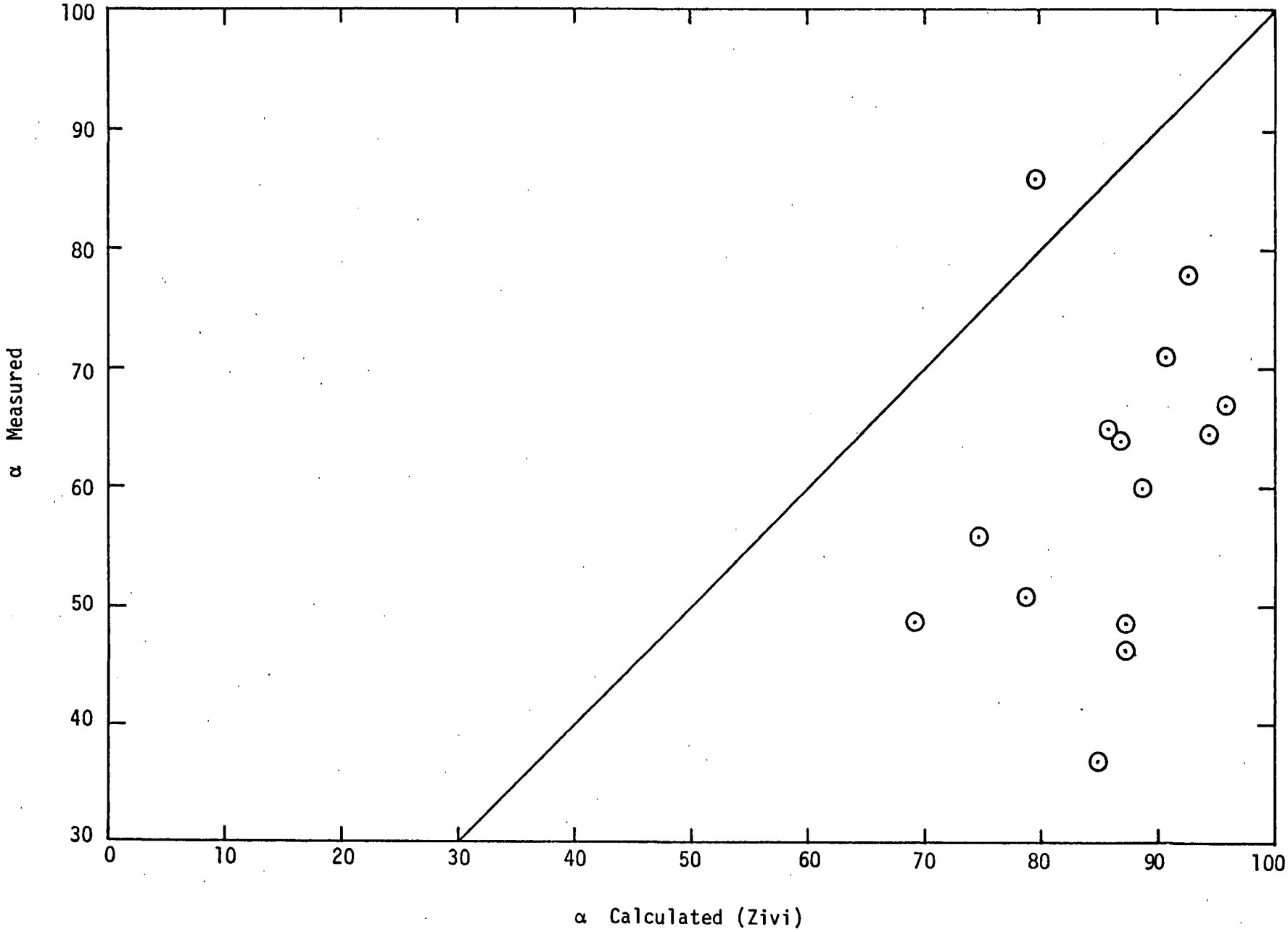

Figure 10. Comparison of void fractions (a) calculated from liquid film thickness measurements and (b) calculated from Zivi's equation and thin-film annular flow model.

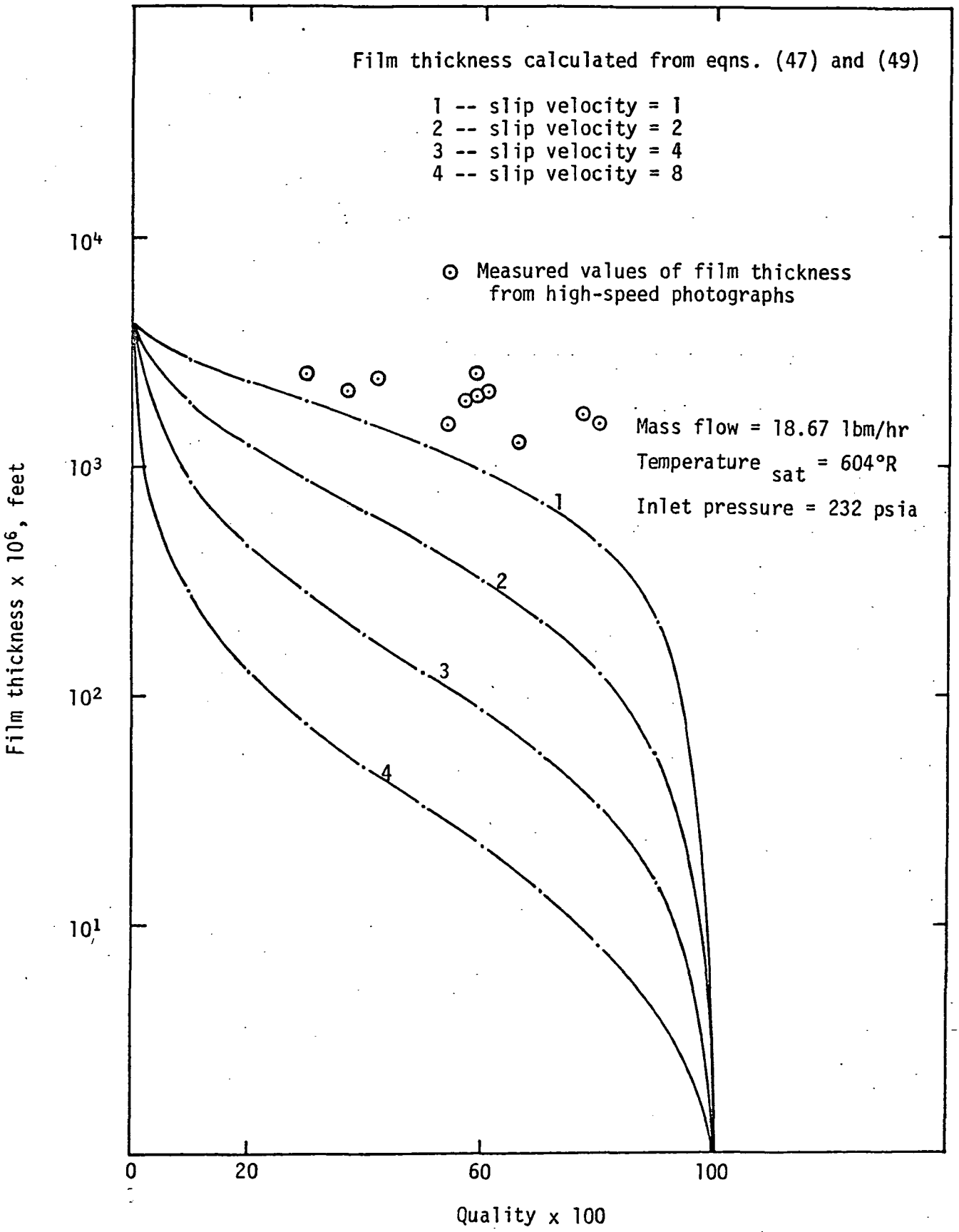

Figure 11. Liquid film thickness at different slip ratios.

equation (47) is based upon a uniform value of δ, whereas in the actual system the gravity-induced drainage from the top of the tube produces unequal film thickness at the top and bottom of the tube.

It was observed that a thin liquid film always wetted the top of the tube wall, and did not appear to change with quality (tube length). Consequently, the measured values of δ were modified in order to correspond more closely to the constant thickness model upon which equation (47) is based. The modification consisted of simply taking one-half of the measured value of δ as the average film thickness about the tube inner periphery, δ_{mod}. This is a conservative approach, as will become apparent in later discussions.

It is immediately observed in table 2 that the calculated values of void fraction from the modified experimental measurements of film thickness are, in all cases except one, considerably lower than those values obtained from the Zivi equation (or from the Martinelli-Nelson results). In other words, the measured film thickness values are much larger than those values to be expected at a given quality. Conversely, if the film thicknesses measured are accurate, and the certainty of this is very high, the values of quality given in reference 3 may be much too high. Another factor that may influence the film thickness value is the slip ratio, V_v/V_ℓ, as indicated in the following equation (ref. 25):

$$\alpha = \frac{1}{1 + \left(\frac{1 - x}{x}\right)\left(\frac{\rho_g}{\rho_\ell}\right) S} \tag{49}$$

where $S = V_v/V_\ell$. This factor is examined in the following section.

Phase velocities.- Indirect, rather than direct, measurements of liquid and vapor velocities in these tests are possible. The experiments conducted were not designed to provide direct measurements, and, consequently, the indirect measurements are to be expected.

Table 2. Comparison of void fractions, (a) calculated from experimental film thickness measurements and eqn. (47), and (b) calculated from Zivi's equation, eqn. (48), and given values of quality (ref. 3).

x (Ref. (3) tests)	δ (Film Meas.) in.	$\frac{1}{2}\left(\delta + \delta_{min}\right)$ in.* δ_{mod}	α (Zivi Eqn.)	α (Eqn. 47, δ_{mod})	Percent Difference
.80	.0187	.0940	.955	.670	29.8
.77	.0202	.0101	.946	.646	31.7
.72	.0122	.0061	.931	.777	16.5
.66	.0160	.0080	.910	.714	21.5
.61	.0232	.0116	.892	.601	32.6
.59	.0247	.0124	.883	.465	47.3
.59	.0310	.0155	.883	.489	44.6
.57	.0209	.0105	.874	.635	27.3
.55	.0401	.0201	.864	.373	56.8
.54	.0200	.0100	.860	.650	24.4
.44	.0072	.0036	.803	.865	-7.7
.42	.0297	.0149	.791	.507	35.9
.37	.0260	.0130	.754	.560	25.7
.30	.0310	.0155	.694	.489	29.5

* δ_{min} assumed zero here.

Indirect measurements of the phase velocities were obtained from (a) frothy, or misty patches of liquid moving through the central vapor-core region at periodic intervals, and (b) disturbances of the liquid interface that appeared to move axially at a steady speed. The former was taken as an indication of the vapor velocity, while the latter was taken as an indication of the liquid velocity. It is obvious that in the case of the former, the velocity of the misty patches is not necessarily equal to the vapor-phase velocity, but may be somewhat lower. Also, in the latter case, the velocity of the disturbance in the liquid layer may likewise not be equal to the true liquid velocity.

The results of these indirect velocity measurements for a few cases are presented in table 1. The velocity measurements were made simply by measuring the distance traveled by some feature within the flow during an interval of many frames, and knowing the associated time interval from timing marks on the side of the 16 mm film. The results obtained are discussed in a later section.

Wavelength.- Measurements were made of the distance between adjacent disturbances in the liquid film, at least one of which continued to grow until it bridged the tube diameter. In the terminology of boiling systems, wavelengths of interest and relevance are the "most dangerous" wavelength--the distance between disturbances that grow most rapidly--and the "critical" or most unstable wavelength--the distance between disturbances most likely to continue growing (see fig. 12). These wavelengths are given by the expressions:

$$\lambda_d = 2\sqrt{3}\,\pi \left[\frac{g_c\,\sigma}{g\,(\rho_\ell - \rho_v)}\right]^{1/2} \tag{50}$$

$$\lambda_c = \lambda_d/\sqrt{3} \tag{51}$$

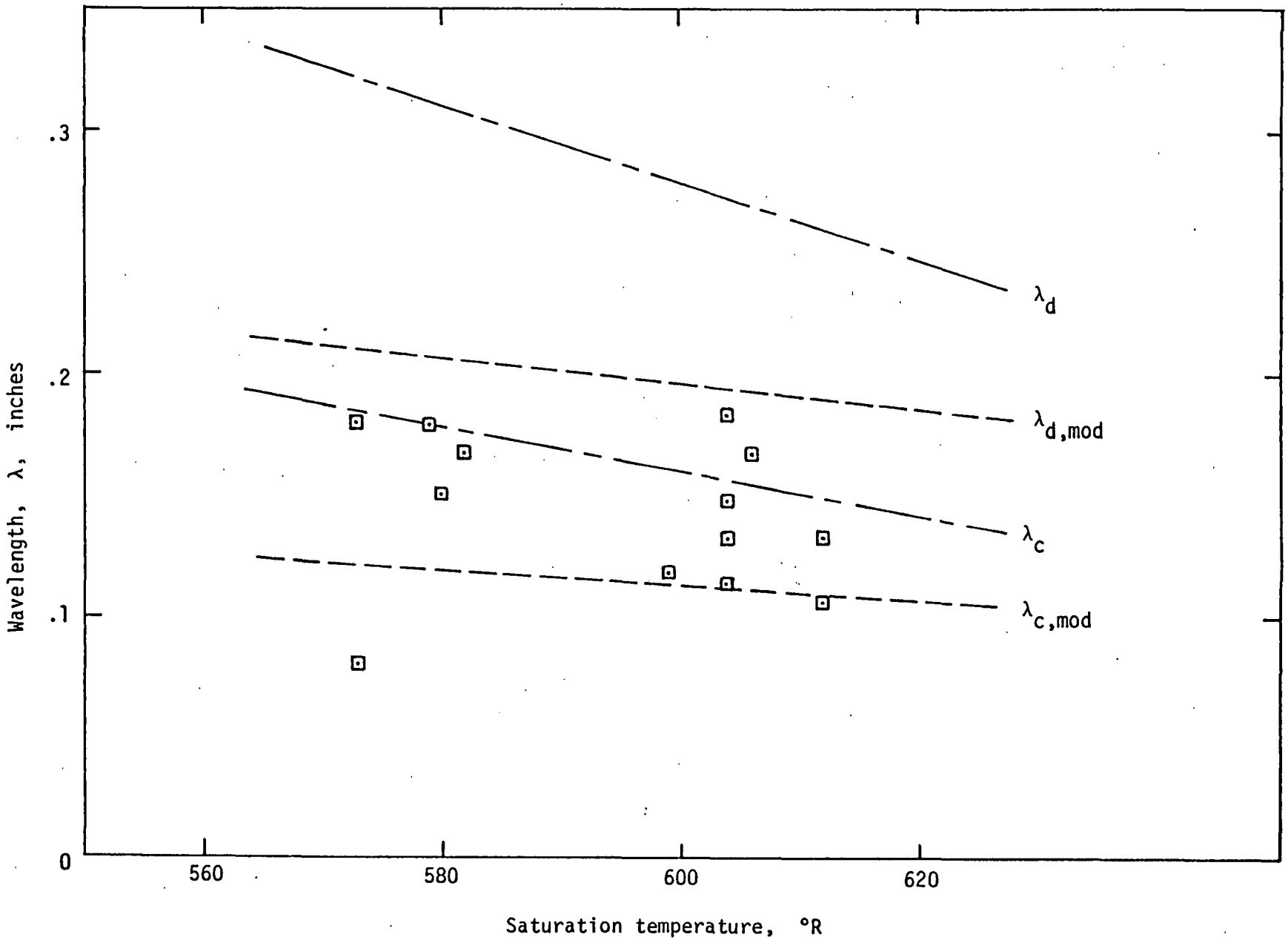

Figure 12. Comparison of measured wavelengths with calculated values of critical and "most dangerous" wavelengths.

Both of the preceding expressions, however, are based upon growth in an infinite plane interface. The present geometry, however, is a tube of quite small diameter. It should therefore be expected that surface tension would have a dampening effect, i.e., restrain the growth of disturbances in the liquid film. Thus, the expressions above should be modified to account for the different wavelength values in a geometry that is influenced to a greater extent by a suppressing surface tension force. An expression that takes into account such effects is as follows (ref. 26):

$$\lambda_{d,mod} = 2\sqrt{3}\,\pi\left[\frac{g}{g_c}\,\frac{(\rho_\ell - \rho_v)}{\sigma} + \frac{1}{(R + \Delta R)^2}\right]^{-1/2} \qquad (52)$$

It should be observed that the second term in the bracket will become dominant for either small diameter systems or in low or zero gravity systems.

A practical consequence of equation (52) is that the wavelengths of the disturbances that may grow in a curved interface will be smaller than those predicted for a flat interface system. Also, in a zero gravity environment the wavelength will be of finite size in a small diameter system. These effects may in turn influence (a) the transition between annular and slug-flow, and (b) system instability, which will be discussed in another section.

Typical values of wavelengths are those for test and run numbers 3-1 and 3-2, where $P = .232$ psia, and $T_{sat} = 144°F$. For these conditions, $\lambda_d = 0.396$ in., $\lambda_c = 0.229$ in., while $\lambda_{d,mod} = 0.293$ in., and $\lambda_{c,mod} = 0.169$ in. The measured values of wavelength are presented in table 1, and appear to fall generally within the region bounded by $\lambda_{d,mod}$ and $\lambda_{c,mod}$, with some indication of a skewing toward $\lambda_{c,mod}$ values.

Flow Instabilities

Condensing instability may be divided into three basic groups as follows:

1. Annular film instability
   (a) gravity-independent instability
   (b) gravity-dependent instability
2. Flow instability (Ledinegg criterion)
3. Vapor-liquid interfacial instability
   (a) plug flow
   (b) droplets striking the interface
   (c) gravity distorting the interface.

Results of the present study have shown that instabilities of type 3 are totally absent from the system tested, and in fact a meniscus per se is not present, i.e., there is no distinct and abrupt change from a totally vapor phase to a totally liquid phase.

Regarding instabilities of type 3(b), the entrainment of liquid drops into the vapor flow will occur if (ref. 27)

$$\frac{\rho_v V_v^2 \lambda}{2\pi\sigma} > 1 \qquad (53)$$

In the present test values of λ ranged from 0.081 to 0.180 inches. Taking a typical run, 3-6, where $\lambda = 0.168$ in., and $V_v = 29.5$ in/sec,

$$\frac{\rho_v V_v^2 \lambda}{2\pi\sigma g_c} = 0.912$$

which indicates conditions near the threshhold of droplet entrainment. This agrees with experimental observations, which indicated relatively little droplet entrainment, the exception being the periodic frothy or misty patches moving at higher velocities than the annular liquid film in the high-quality annular flow regions.

The instabilities of type 1-(a) are those manifested by the formation of waves on the surface of the liquid film, due to relative

motion of the two phases. As these waves grow, the shearing action of the waves will tend to force the wave crests to bridge the tube diameter, resulting in alternate pockets of liquid and vapor. This constitutes the transition from annular to slug flow, each region having different flow and pressure drop characteristics, thus presenting a possible source of flow instability. This process was observed frequently. The previous section dealing with wavelengths indicates that even under zero-g conditions such instabilities may occur in small diameter systems.

The dimensionless parameters governing this type of instability (see Miles, ref. 28) are the Weber and Reynolds numbers,

$$We = \frac{\rho_\ell V_i^2 \delta}{\sigma g_c} \tag{54}$$

$$Re_\delta = \frac{\rho_\ell V_i \delta}{\mu_\ell} \tag{55}$$

Calculations of Re_δ and We based upon the experimental measurements obtained here, and presented in table 1, are presented in table 3. Comparison with the Miles stability criteria is illustrated in figure 13. The calculated values of Re_δ and We must be considered approximate due to the inability to measure liquid and vapor velocities accurately.

Regarding gravity-related film instability (or liquid runback instability) such as type 1-(b), such instabilities may be present in vertically oriented systems, and in fact, can affect condenser performance appreciably (ref. 11). However, no such instabilities are observable in a horizontally oriented system as in the present tests. Furthermore, under zero-g conditions the vapor shear force would be infinitely large compared with the gravity force acting on the liquid film, and thus this type of instability would not exist in a zero-g environment.

Finally, the instability of type 2 would be expected to occur in a high-heat flux system, i.e., if

Table 3. Calculated values of various dimensionless numbers, based upon experimentally measured quantities.

Run No.	T_{sat} (°F)	δ (in.)	V_v (in./sec)	V_ℓ (in./sec)	We (1)	Re_δ (1000)	Fr (1)	Fr/Re_δ (10^{-3})	Bo (1)
4-2	119	.0202	30.0	20.0	26.6	1370	4.52	3.30 (10^{-3})	.520
4-3	120	.0264	32.9	21.9	42.3	1960	4.15	2.12 (10^{-3})	.896
4-4	119	.0247	20.8*	13.9	15.6	1160	1.83	1.58 (10^{-3})	.777
4-5	122	.031	20.8	13.9	20.2	1450	1.43	.98 (10^{-3})	1.26
4-8	139	.0297	33.6**	22.4	61.3	2250	3.94	1.76 (10^{-3})	1.40
4-9	139	.0187	33.6**	22.4	38.6	1420	6.26	4.41 (10^{-3})	.556
3-1	144	.0072	33.6	22.4	15.9	545	16.4	30.0 (10^{-3})	.088
3-2	144	.016	33.6**	22.4	35.4	1210	7.36	6.06 (10^{-3})	.436
3-3	144	.026	28.0	18.7	39.9	1640	3.16	1.92 (10^{-3})	1.15
3-6	146	.0401	29.5	19.7	70.2	2660	2.28	.86 (10^{-3})	2.82
3-10	145	.0122	33.6**	22.4	27.7	925	9.68	10.4 (10^{-3})	.257
3-11	144	.0232	28.0*	18.7	35.6	1465	3.54	1.07 (10^{-3})	.916
3-12	145	.0209	28.0*	18.7	32.5	1320	3.94	2.98 (10^{-3})	.755

* same velocity as in run 4-5 assumed

** same velocity as in run 3-1 assumed

Critical values of dimensionless force ratios shown in parentheses (ref. 42).

$We = \rho_\ell V_\ell^2 \delta / \sigma g_c$; $Re_\delta = \rho_\ell V_\ell \delta / \mu_\ell$; $Bo = g\rho_\ell \delta^2 / g_c \sigma$;

$Fr = \rho_\ell V_\ell^2 / g \sin\theta \, (\rho_\ell - \rho_v)\delta$.

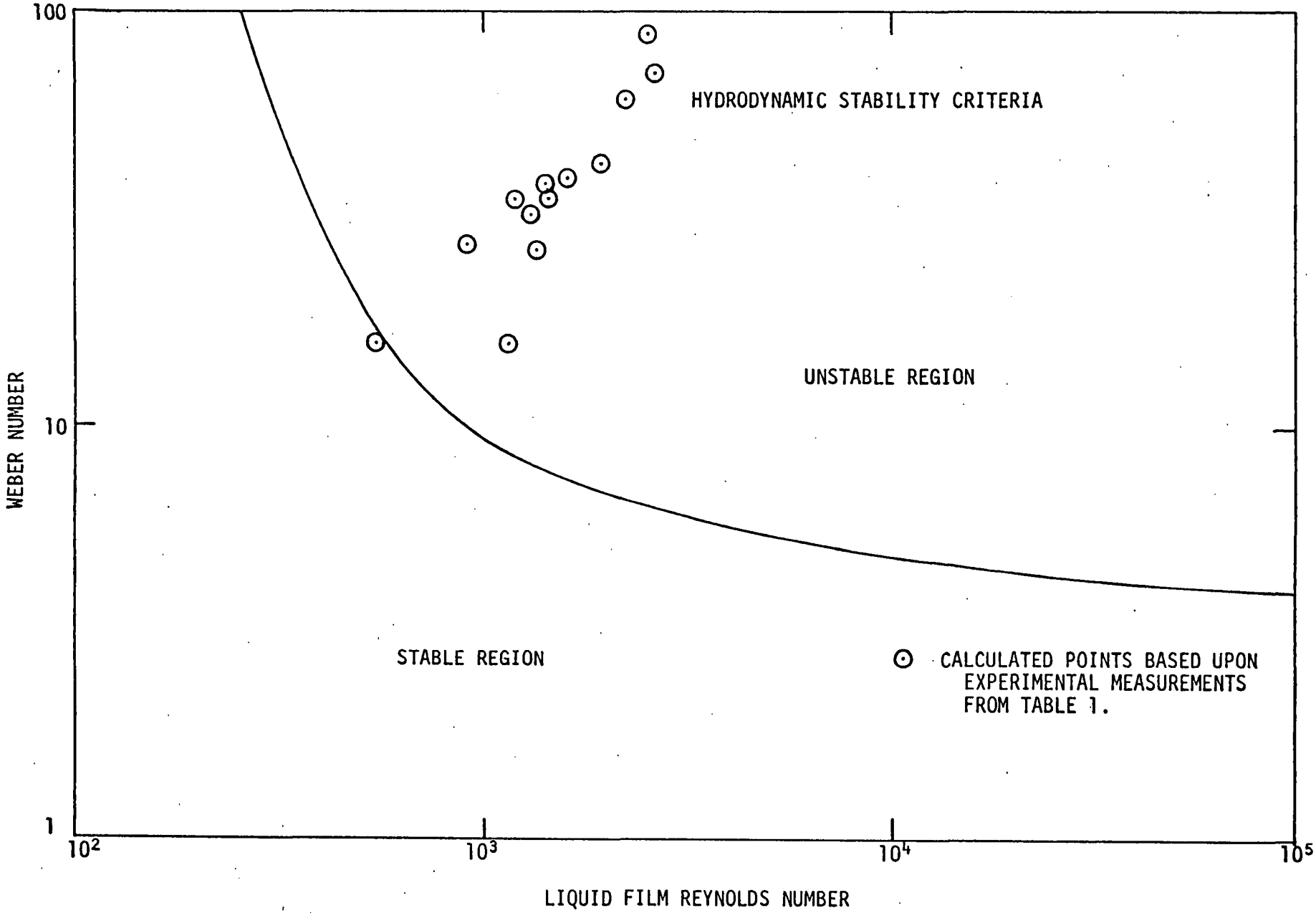

Figure 13. Annular flow stability domains.

$$\frac{q}{A} > \frac{\lambda}{4} \left[3\, G_T f_v + \frac{g \rho_\ell \rho_v D}{G_T} \right] \qquad (56)$$

For the present test conditions q/A calculated from equation (56) is about $4(10^5)$ BTU/hr-ft^2, whereas the actual maximum heat flux in the system was only about 10^4 BTU/hr-ft^2. Consequently, instabilities of this type should not be expected in the present condensing system under either 1-g or 0-g conditions. Certainly all observations under 1-g conditions for the present tests indicated no such instability. That is, the location of the point of complete vapor extinguishment in the three transparent tubes remained very steady, even under the highest flow rates and inlet temperature levels. Also, no oscillatory behavior (parallel channel instabilities) of the points of complete condensation were ever observed to occur.

Consequently, it appears that the only potential system instability for a condensing system of this type would be that of type 1-(a). Additional discussion of instabilities is found in Appendix A.

The various types of instabilities which may occur are a result of an imbalance of the fundamental forces operative in the particular system. Stability criteria, then, are based upon the relative magnitudes, or ratios of these forces, as described earlier. Due to the lack of 0-g data, and due to the lack of accurate 1-g results (gross inaccuracies in quality values to be discussed later), such stability criteria could not be established or verified experimentally. Alternatively, however, the various operative forces have been computer calculated and various significant dimensionless ratios evaluated for a condensing system. Such results are presented in figures 14 through 19. Experimental establishment of the values of these ratios at the onset of the various types of instabilities with the results available is not possible.

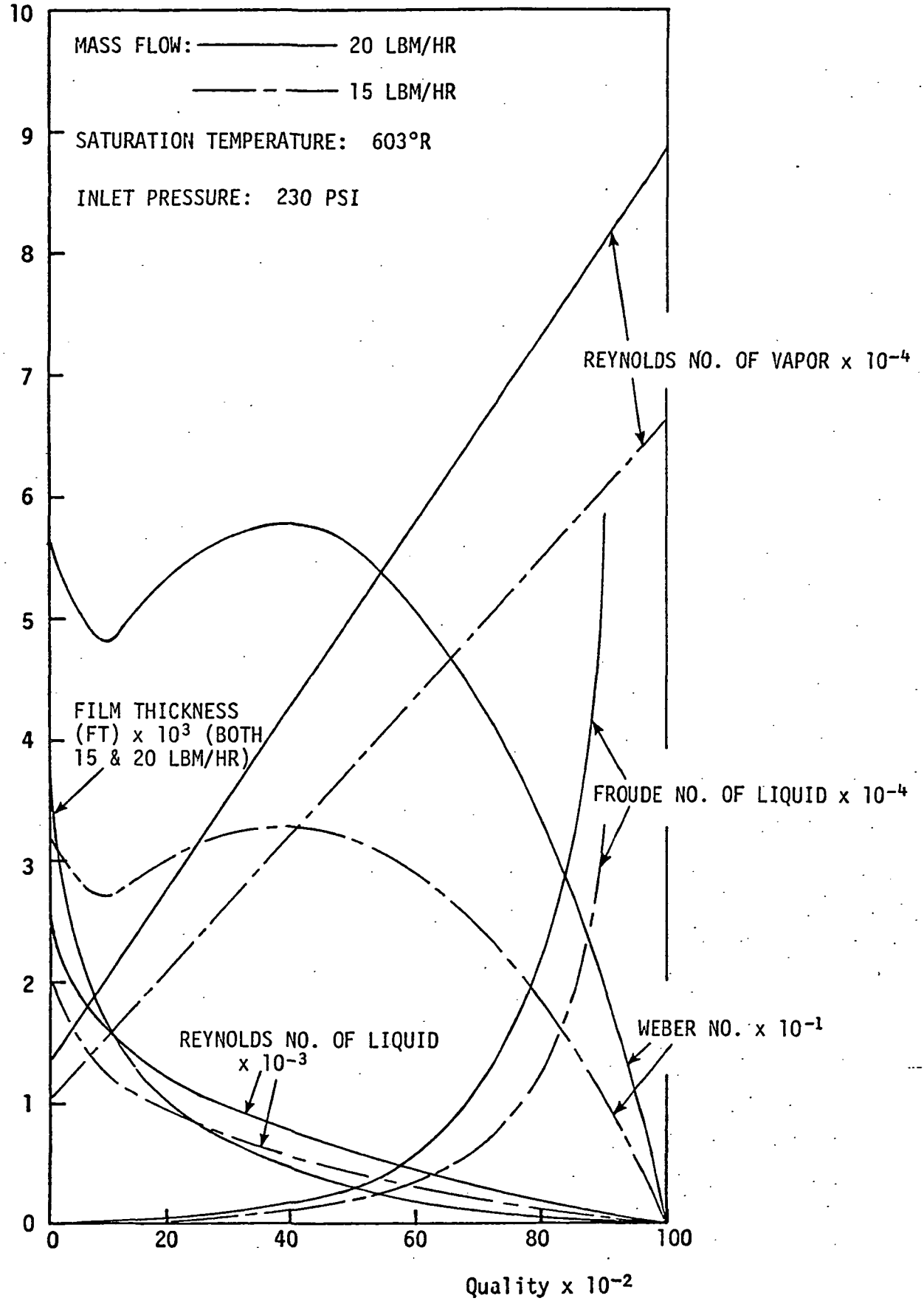

Figure 14. Liquid and vapor Reynolds number, Froude number, and film thickness, $\dot{m}$ = 20 lbm/hr.

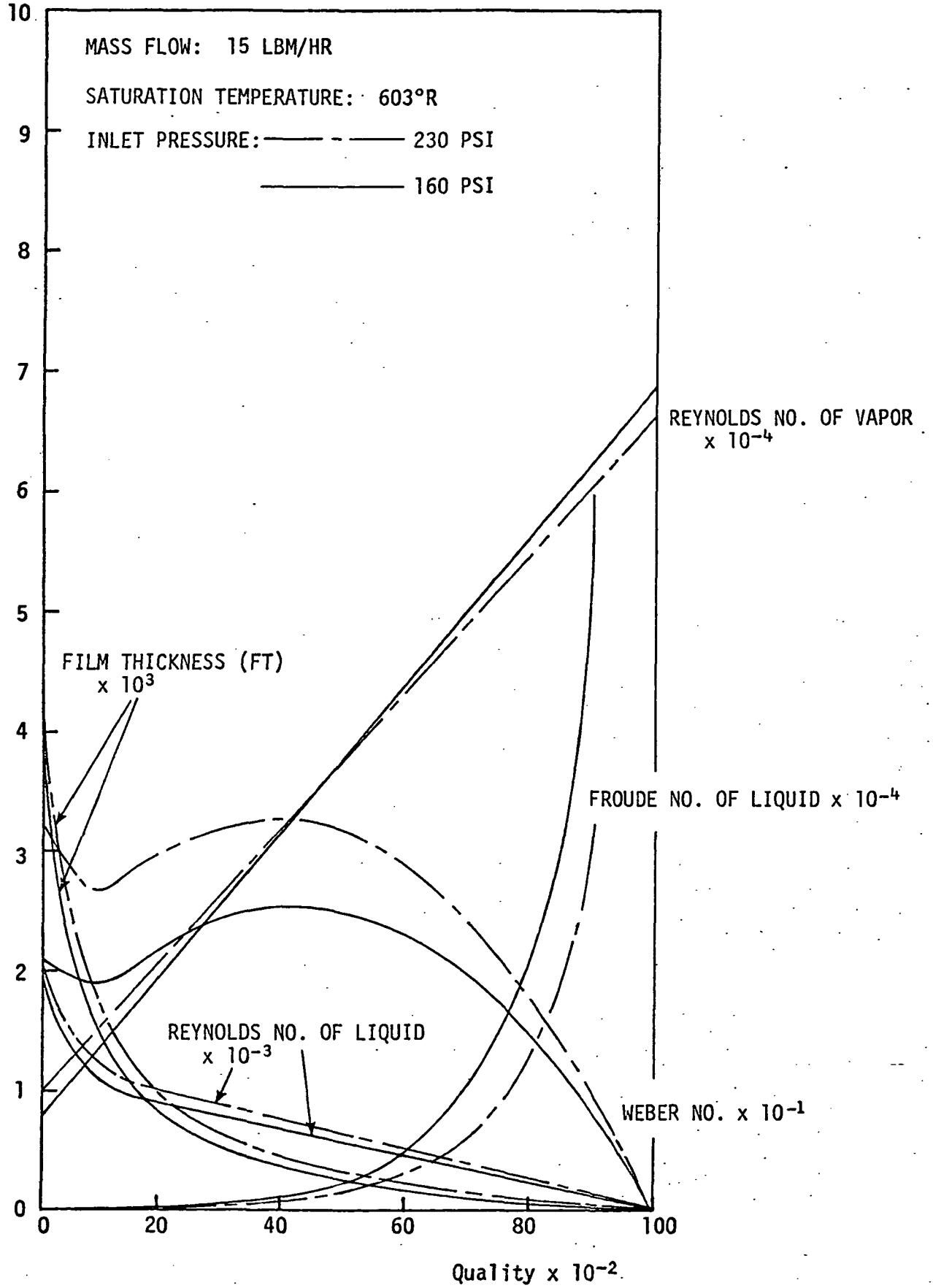

Figure 15. Liquid and vapor Reynolds number, Froude number, and film thickness, $\dot{m}$ = 15 lbm/hr, different pressures.

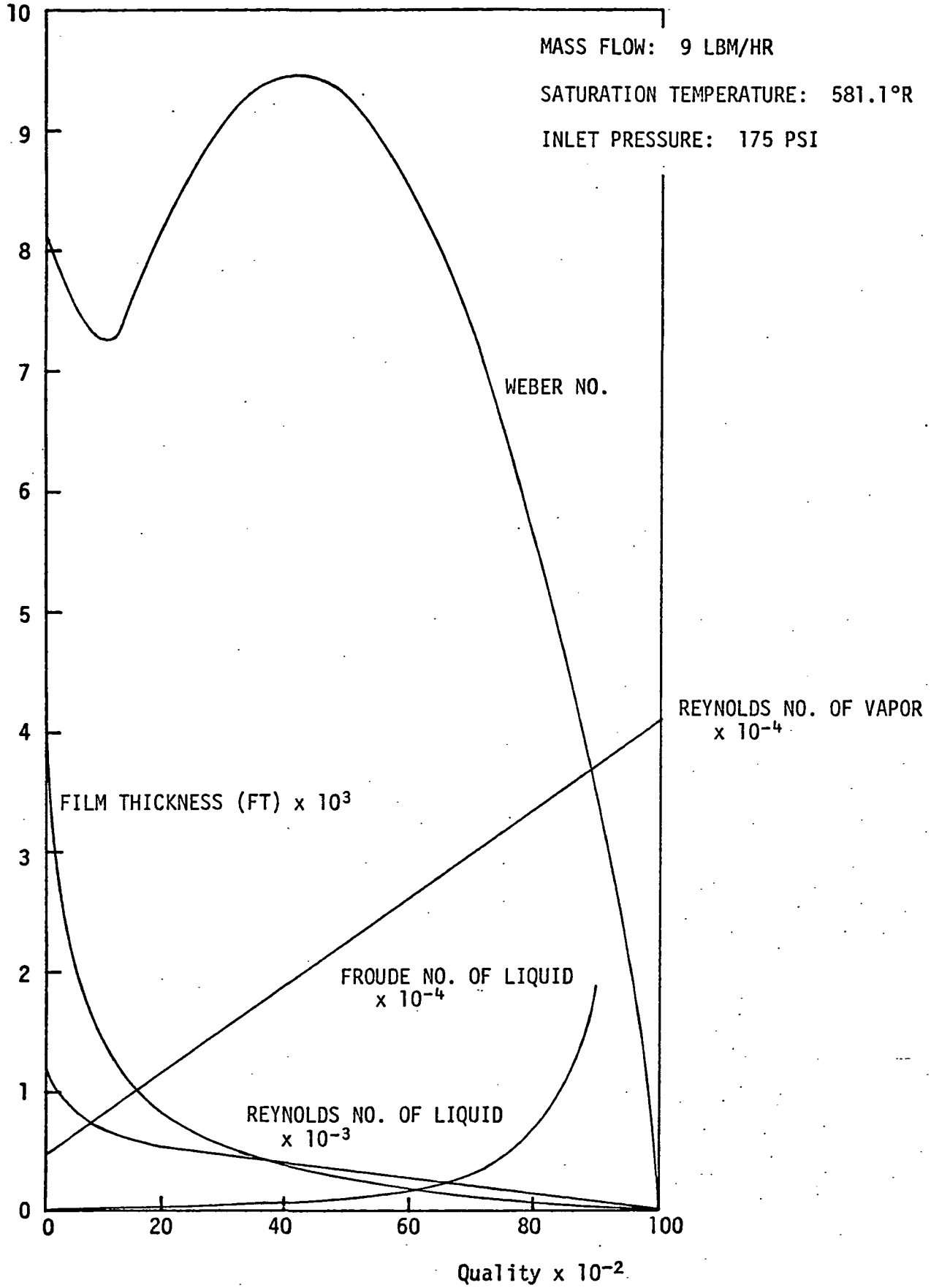

Figure 16. Liquid and vapor Reynolds number, Froude number, and film thickness, $\dot{m}$ = 9 lbm/hr, 175 psia.

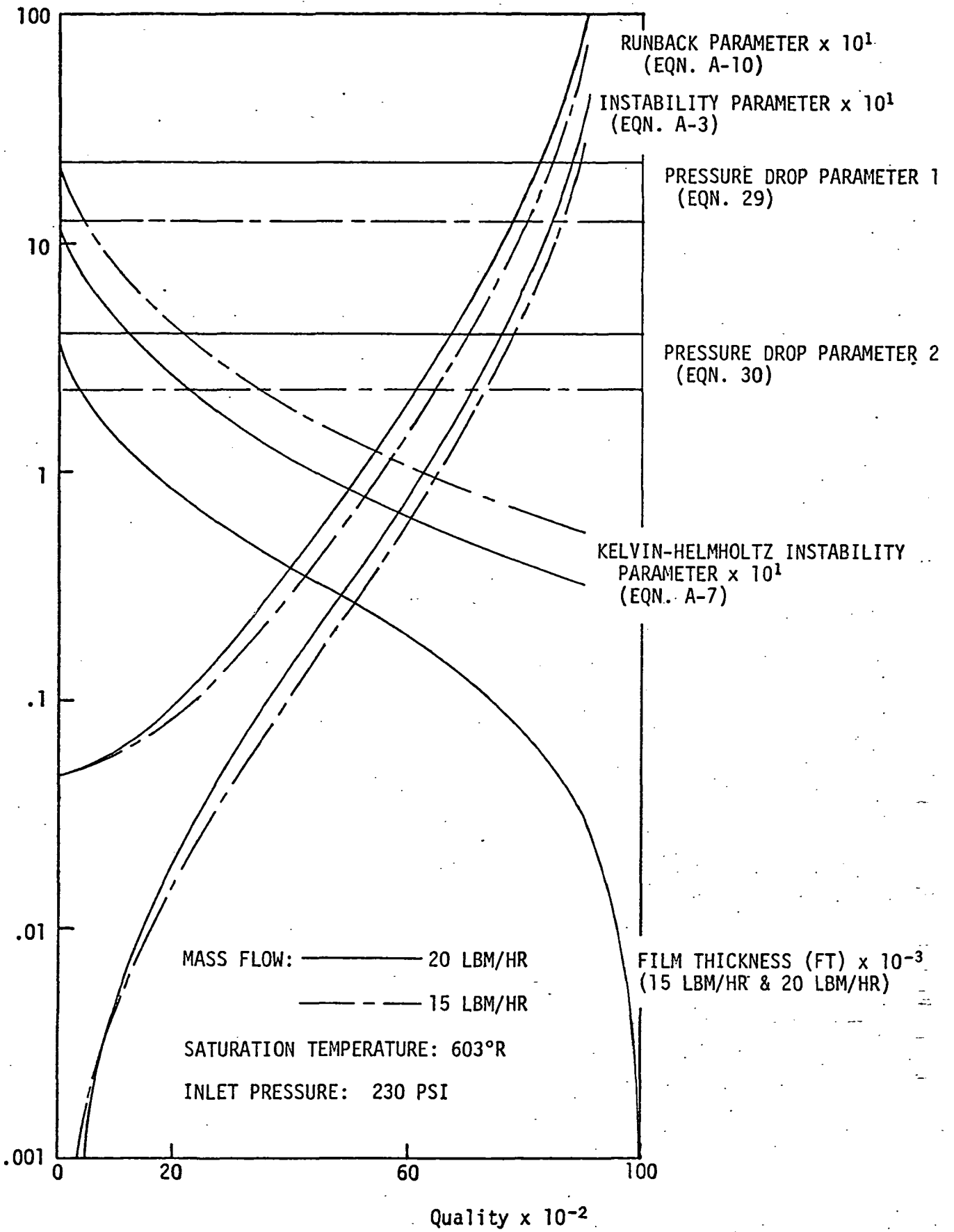

Figure 17. Instability parameters, $\dot{m}$ = 20 lbm/hr, 230 psia.

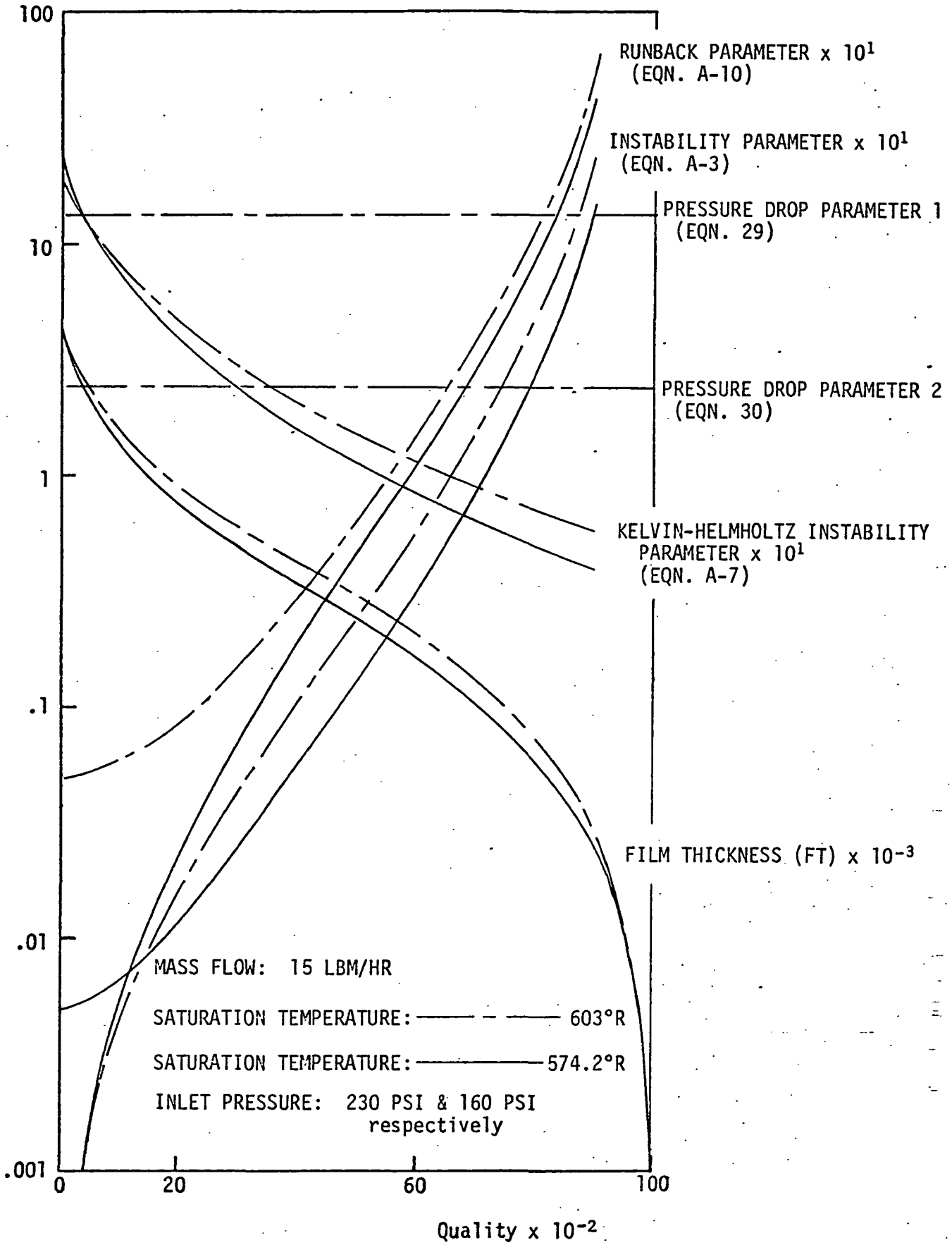

Figure 18. Instability parameters, $\dot{m}$ = 15 lbm/hr, different pressures.

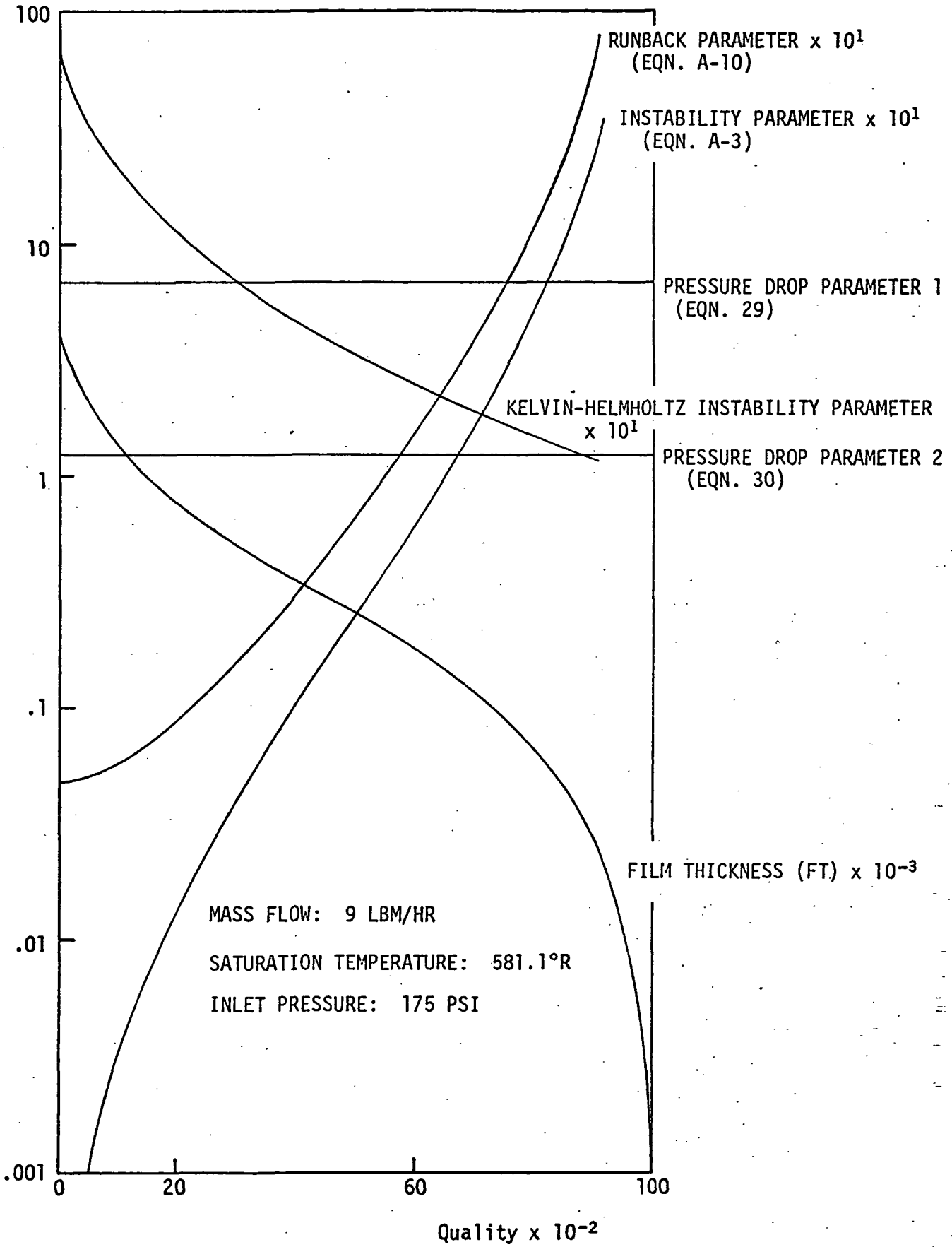

Figure 19. Instability parameters, $\dot{m}$ = 9 lbm/hr, 175 psia.

HEAT TRANSFER MODEL

A model for predicting heat transfer coefficients, local and total heat fluxes, and condensing lengths in a flow condensation system under 1-g conditions is presented in Appendix B. This model served as the basis for the results obtained in reference 29. It is necessary to modify this model to account for differences due to 0-g operation; specifically, hydrodynamic differences in the two-phase region which may affect heat transfer characteristics. It is the objective of this section to modify the model so as to take into account the flow differences observed in the limited amount of 0-g data (qualitative) obtained, and estimate the differences in heat transfer that occur as a result of the change of flow pattern.

The model is modified by assuming a symmetrically centered vapor core in a 0-g environment, while the vapor core and bubbles under 1-g conditions are displaced upward at the top of the tube. Only an annular flow region is assumed to exist in the two-phase region. This appears justified in view of the results of figure 9, especially since the values of quality presented in the ground tests (ref. 3) appear high by 20 to 30 percent at the inlet. Also, in the stratified-wavy-annular region, and in the elongated bubble and slug flow regions, the same general type of upward displacement occurs. Only the size of the vapor core changes (or alternatively, the thickness of the liquid film about the tube inner periphery). That is, an approximation to the film thickness under 1-g conditions would be a linear variation from 0 at the top of the tube (0°) to δ_{max} at the tube bottom (180°), or $\delta = (\delta_{observed}/\pi)\theta$. In the 0-g case, δ would simply remain constant.

The heat transfer coefficient for annular flow (ref. 30) is given by

$$\frac{h}{h_\ell} = a\left(\frac{1}{X_{tt}}\right)^b \qquad (57a)$$

where $$X_{tt} = \left(\frac{\mu_\ell}{\mu_g}\right)^{0.1} \left(\frac{\rho_g}{\rho_\ell}\right)^{0.5} \left(\frac{1 - x}{x}\right)^{0.9} \qquad (57b)$$

and $a = 3.5, \quad b = 0.5$ (Dengler and Addams)

or $a = 3.4, \quad b = 0.45$ (Guerreri and Talty)

or $a = 2.5, \quad b = 0.7$ (Collier and Pulling)

Now relating x to film thickness δ, from Zivi's void fraction expression,

$$\frac{1 - x}{x} = \left(\frac{1 - \alpha}{\alpha}\right)\left(\frac{\rho_\ell}{\rho_v}\right)^{2/3} \qquad (58)$$

but from equation (47)

$$\alpha = 1 - 4\,\frac{\delta}{D} + 4\left(\frac{\delta}{D}\right)^2 \qquad (59)$$

and

$$\frac{1 - x}{x} = \frac{4\,\frac{\delta}{D}\left(1 - \frac{\delta}{D}\right)}{1 - 4\,\frac{\delta}{d} + 4\left(\frac{\delta}{D}\right)^2} \quad \frac{\rho_\ell}{\rho_v}^{2/3} \qquad (60)$$

Now for the special case of $\delta << D$ (which is not a good assumption at low qualities)

$$\left(\frac{\rho_v}{\rho_\ell}\right)^{2/3} \frac{1 - x}{x} \approx \frac{4\,\frac{\delta}{D}}{1 - 4\,\frac{\delta}{D}} \approx 4\,\frac{\delta}{D} \qquad (61)$$

thus $$X_{tt} = \Gamma \left(4\,\frac{\delta}{D}\right)^{0.9} \quad \frac{\rho_\ell}{\rho_v}^{0.6} \qquad (62a)$$

where

$$\Gamma = \left(\frac{\mu_\ell}{\mu_g}\right)^{0.1} \left(\frac{\rho_g}{\rho_\ell}\right)^{0.5} \tag{62b}$$

and so

$$\frac{h}{h_\ell} = \frac{a}{\Gamma^b \, 4^{0.9b}} \left(\frac{D}{\delta}\right)^{0.9b} \left(\frac{\rho_v}{\rho_\ell}\right)^{0.6b} \tag{63}$$

Using the Collier and Pulling values of a and b,

$$\frac{h}{h_\ell} = \frac{1.044}{\Gamma^{0.7}} \left(\frac{1}{\delta/D}\right)^{0.63} \left(\frac{\rho_v}{\rho_\ell}\right)^{0.42} \tag{64}$$

Now if

$$\delta_{act} = \delta_{obs} \left(\frac{\theta}{\pi}\right) \tag{65}$$

or

$$\frac{\delta_{act}}{D} = \frac{\delta_{obs}}{D} \left(\frac{\theta}{\pi}\right) \tag{66}$$

for 1-g conditions

$$\left(\frac{h}{h_\ell}\right)_{1\text{-}g} = \frac{1.044}{\Gamma^{0.7}} \left[\frac{1}{\left(\frac{\delta_{obs}\,\theta}{\pi D}\right)}\right]^{0.63} \left(\frac{\rho_v}{\rho_\ell}\right)^{0.42} \tag{67}$$

To compare 1-g and 0-g heat transfer coefficients one must determine an average heat transfer coefficient,

$$h_{avg,1-g} = \frac{\int_o^{\pi} h(\theta)\, r\, d\theta}{\int_o^{\pi} r\, d\theta} = \frac{h_\ell \int_o^{\pi} \frac{1.044}{\Gamma^{0.7}} \left(\frac{\pi D}{\delta_{obs}\,\theta}\right)^{0.63} \left(\frac{\rho_v}{\rho_\ell}\right)^{0.42} r\, d\theta}{\int_o^{\pi} r\, d\theta} \tag{68}$$

$$h_{avg,1-g} = 0.684\, \frac{h_\ell}{\Gamma^{0.7}} \left(\frac{D}{\delta_{obs}}\right)^{0.63} \left(\frac{\rho_v}{\rho_\ell}\right)^{0.42} \int_o^{\pi} \frac{1}{\theta^{0.63}}\, d\theta$$

or (69)

$$\frac{h_{avg,1-g}}{h_\ell} = \frac{2.82}{\Gamma^{0.7}} \frac{1}{\left(\frac{\delta_{obs}}{D}\right)^{0.63}} \left(\frac{\rho_v}{\rho_\ell}\right)^{0.42}$$

for a particular axial location.

Comparing equation (69) with the 0-g case (uniform δ), δ for the corresponding 0-g case would be $(\delta_{obs}/2)$ for the linear variation of δ with θ used here. Consequently,

$$\left.\frac{h}{h_\ell}\right)_{0-g} = \frac{2.5}{\Gamma^{0.7}} \left(\frac{1}{4\ \frac{\delta_{obs}}{2D}}\right)^{0.63} \left(\frac{\rho_v}{\rho_\ell}\right)^{0.42} \tag{70}$$

or

$$\left.\frac{h}{h_\ell}\right)_{0-g} = \frac{1.615}{\Gamma^{0.7}} \frac{1}{\left(\frac{\delta_{obs}}{D}\right)^{0.63}} \left(\frac{\rho_v}{\rho_\ell}\right)^{0.42} \tag{71}$$

and so

$$\frac{h_{0\text{-}g}}{h_{avg,1\text{-}g}} = \frac{1.615}{2.82} = 0.573 \tag{72}$$

It therefore appears that, according to this model, heat transfer for a uniform film thickness (0-g conditions) is not as effective as that for a non-uniform film thickness, as under 1-g conditions, for any given axial location. It should be emphasized that these results are based upon $\delta << D$, which is not true for low quality regions.

DISCUSSION OF RESULTS

Flow Regimes

Whether the Baker chart can be employed to adequately predict flow regimes in a very small diameter condensing flow system, similar to the present study, is actually somewhat doubtful. Initial doubts are raised whenever it is realized that Baker's original map was based upon adiabatic two-component two-phase flows in large diameter horizontal pipes at atmospheric pressures, resembling the present study only in the two features "two-phase" and "horizontal". While the photographic observations obtained herein agree reasonably well with the Baker map predictions (see fig. 8), the number of data points is not so large as to define with certainty any new boundaries, or to shift the original flow regime boundaries.

In a similar study of condensing refrigerant-12 and -113 flows in horizontal tubes, ranging from 0.1875 in. to 0.625 in. diameter, it was found that Baker's map was inadequate (ref. 31). Instead, new boundaries were drawn on the map that described the flow pattern transitions more accurately. These new boundaries were based on a large and broad amount of data.

It is of interest to note in the same paper (ref. 31) that flow pattern maps for a particular diameter tube (3 in all) and for

either fluid, attempts to combine the results of even a single fluid for different diameter tubes, or for two fluids in the same diameter tube, were unsuccessful. An alternative flow pattern map was presented that correlated the data well when plotted on the basis of liquid velocity and $(1 - \alpha)/\alpha$. This map could be of value principally because flow regime predictions appear not to be dependent upon fluid properties or tube diameter, but only upon liquid velocity and void fraction. This is perhaps a result of the void fraction being calculated from an expression developed by Smith (ref. 32) that was based upon a large body of experimental data of several different investigations, and was shown to be valid for all flow conditions of concurrent two-phase flow, irrespective of flow pattern, mass velocity, dryness fraction, or pressure. It appears that this newly proposed map warrants further interest and examination.

Perhaps the most significant finding of the present study with respect to flow regimes is that such a large fraction of the flow is in the annular, annular-stratified, or annular-wavy regions (fig. 9). Since later discussion will indicate that the quality measurements are too high--in some cases by about 30 percent--an even larger fraction of the flow is annular in character than that indicated by figure 9. This finding makes the heat transfer analysis and predictions of Bae, et al. (ref. 16) quite attractive in predicting heat transfer behavior of similar systems since it is based almost entirely upon an annular flow model.

It is also of passing interest to note that the heat transfer-flow model proposed, before any experimental results were obtained, to predict the heat transfer behavior of the present condenser systems was also a fully annular flow model (in the two-phase region). The results obtained using that model were found to correlate with test data "to probably better than ± 20 percent" (ref. 29). It was concluded that the computer program developing using the model supplied could "be used with confidence to predict test results and analyze test data" (ref. 29).

Based upon the verification of the existence of a preponderantly annular flow, a modification to the basic model was made herein to attempt to estimate 0-g effects, and is discussed later.

Film Thickness, Quality and Void Fraction

The large discrepancy between void fractions calculated from (a) experimental measurements of film thickness, and (b) Zivi's equation, is evident in figure 10. In view of the past success of the Zivi equation (ref. 10) it is reasonable to estimate or check those values calculated from the experimental measurements.

If one chooses arbitrarily a void fraction of 0.90, the corresponding film thickness, from equation (47), is 0.0026 in. At $\alpha = 0.90$, $x \approx 0.65$, and in examining the measured values of δ at qualities in the vicinity of 0.65 in table 2, the modified measured values of δ are roughly between 2.5 and 6.0 times as large. Or from another viewpoint, the modified measured values of film thickness correspond to qualities which are about 30 percent lower than those values presented with the raw test data in reference 3.

This is indicated visually by both figures 10 and 11. In figure 10 it appears that a shift of all data points to lower quality values of 30 percent would produce a reasonable distribution about the line of predicted values. The scatter of the data, per se, is quite large, which seems to be another indication of the lack of reliability of the quality values obtained in the ground tests (reference 3).

In figure 11 a shift of data also appears appropriate. That is, the measured values of liquid film thickness are considerably larger than that predicted by equations (47) and (49). Actually, the two comparisons, figures 10 and 11, are equivalent comparisons, but figure 11 shows additionally that even in the case of unequal liquid and vapor velocities, i.e., for higher slip ratios than unity, the disagreement still exists, and in fact, the disagreement is even more severe.

It therefore appears that the quality values obtained in ground tests (ref. 3) were in error, and the various measurements obtained in the present tests consequently cannot be meaningfully correlated with quality. This conclusion regarding the quality

measurement agrees with later operational testing, and modification of the system at NASA-JSC. It was concluded that the quality measurements in question were inaccurate and invalid since the original instrumentation indicated inlet temperatures that were actually quite far upstream of the condenser panel(s) inlet (ref. 33). That is, an indication of vapor temperatures at saturation conditions actually meant that considerable condensation occurred before the inlet to the condenser panel tubes. This also explains the initial inability to obtain agreement between measured and computed values of distances required for complete condensation within the condenser tubes in reference 29. In reference 29 it was speculated that this discrepancy might have been due to an additional heat leak from the condensing system, and indeed, partial condensation before the inlet to the test section is equivalent to a large heat leak.

Phase Velocities

As in the previous section, if one attempts to check the accuracy of the velocity measurements assuming quality (or void fraction) values to be accurate, unrealistic results are obtained.

From continuity,

$$W = W_v + W_\ell \tag{73}$$

$$W = \rho_v V_v A \alpha + \rho_\ell V_\ell A (1 - \alpha) \tag{74}$$

or

$$G = \rho_v V_v \alpha + \rho_\ell V_\ell (1 - \alpha). \tag{75}$$

Taking the measured values from test 3-6, table 1, and using figure 2.6 in reference 9 to obtain α from the given quality values, V_ℓ is required to be 88.6 in./sec if the measured vapor velocity, V_v, is accepted as accurate. It is hardly likely that the liquid phase velocity is larger than the vapor phase velocity. Conversely,

if the measured value of V_ℓ is accepted, then V_v is required to be 131 in./sec, which is over 4 times as large as the measured velocity of the frothy patches. While this is possible, it again appears to be improbable, as implied by figure 11.

Viewed from a different perspective, one might calculate the value of quality that should produce velocity values in reasonable agreement with those measured. If one accepts values of V_v and V_ℓ of 29.5 and 20.1 in./sec, respectively, one finds α must be 0.412, which corresponds to a quality of less than 0.1. This is only one-fifth as large as the given test value--once again an unreasonably large discrepancy.

Additionally, if one assumes that the quality is not .55, but .30 less, as previously discussed, and assumes equal liquid and vapor velocities, then $V_v = V_\ell \approx 40$ in./sec, which is in much better agreement with the photographically measured velocities. Even though the measured velocities are smaller, it would be expected that the velocities of the frothy patches and the liquid film disturbances would be less than the true vapor and liquid velocities respectively.

Finally, if one calculates the magnitudes of the Mach number, using the mass flow rates and pressures given for each test run (ref. 3), it is found that unrealistic values are obtained in most cases, i.e., $M_o > 1$. Since supersonic flow conditions cannot exist in the condenser tubes, it again appears likely that condensation occurred prior to the test section inlet, resulting in an average mixture density larger than that of the vapor phase alone, which would produce calculated values of $M_o < 1$, in accord with reality.

Wavelength

The measurements of wavelength obtained here agree well with the predictions of equation (52), as seen in figure 12. The practical significance of these results is believed two-fold.

First, it does appear that interfacial and system instabilities are possible in two-phase radiator/condenser systems having

small diameter flow channels, even under conditions of zero gravity. Equations (50) and (51) predict an infinite wavelength, or an infinite distance between disturbances in a 0-g environment. However, the second term in equation (52) predicts a finite disturbance interval in a 0-g environment that is related to the curvature of the flow channel. The experimental measurements appear to substantiate the presence and accuracy of the wall curvature effect, even though the tests occurred under 1-g conditions. The effect was observable, in other words, even in a 1-g environment, because of the small diameter of the condensing tube.

If a finite wavelength is to be expected, then a perfectly stable, smooth interface will not exist in a completely annular flow condition under 0-g conditions. Therefore, a transition to slug flow is a possibility under certain conditions, and consequently pressure drop and heat transfer may not be predicted accurately using a highly idealized flow model. The conditions under which a transition(s) may occur should be further investigated. That is, effects of tube diameter, liquid-solid wetting characteristics, and destabilizing liquid-vapor interfacial shearing actions should be considered further in modeling 0-g behavior.

Secondly, it does appear from the limited data available that the critical wavelength is of practical significance, rather than the most dangerous wavelength. This is especially reasonable in a low-flux heat level system, as opposed to a high-heat flux boiling system near the critical heat flux, where the most dangerous wavelength has proved a meaningful concept in predicting the critical heat flux (ref. 34).

Flow Instabilities

From information and discussions appearing earlier in this report, parallel channel instability does not appear to be a potential problem, as indicated by the Ledinegg criterion. The maximum system heat flux in the present system was less than

3 percent of that producing instability, according to equation (56). Furthermore, under space environment conditions the limiting factor on heat flux is likely to be the thermal resistance associated with radiation to the environment, which makes it unlikely that the limits of equation (56) will be exceeded.

It does appear that gravity-independent instabilities, such as those resulting in the formation and growth of waves, as in an annular film, must be examined further. It appears possible that wave formation is a possibility under zero-g conditions, even though surface tension has a stabilizing effect on the liquid annular film. This possibility appears to be substantiated by equation (52) and the experimental results presented herein.* The particular instability parameters that appear governing in this instance are the Weber number, which represents the ratio of inertial and surface tension forces, and the Reynolds number (inertial forces/viscous forces).

The stability analysis of Miles (ref. 28) thus appears to be of greatest practical significance, and indeed, was one of the criteria upon which the present r/c panel design was based (ref. 17). Miles determined that for large liquid Reynolds numbers ($Re \to \infty$), a sufficient condition for stability is that the Weber number be less than 3, while at Reynolds numbers lower than 200, the flow will be stable for any Weber number. Accurate experimental measurements obtained under 1-g and 0-g conditions are needed to verify these conditions for stable flow.

In calculating the magnitudes of We and Re from the measurements listed in table 1, and plotting these values on the Miles stability diagram of figure 13, it appears that all measured

---

* For very small tube diameters, the wavelength spacing is so small that disturbances will be damped out by the fluid. That is, the flow will be stabilized by the surface tension and viscous damping forces of the fluid itself.

data points (except one) indicate an unstable liquid-vapor interface. This is not quite in agreement with experimental observations. That is, while wave formation did occur, very little droplet entrainment did.

Part of the reason why the points fall above the boundary, even though the system was designed to operate below the boundary in the stable region, is that liquid drainage from the top of the tube resulted in a film thickness essentially double that expected assuming an idealized uniform annular film model, which was the basis of design calculations. A doubled film thickness results in Weber numbers being larger by a factor of 4, while the Reynolds numbers are simply doubled. Also, it should be kept in mind that the measured velocities cannot be considered high-accuracy measurements, since wave movement and entrained droplet movements are not necessarily the same as the liquid and vapor velocities.

Thus, both Re_δ and We are larger than those values expected to exist in the idealized annular flow configuration, i.e., under 0-g conditions. Consequently, testing under 1-g conditions for flow instability is a more stringent, more conservative test. That is, if 1-g tests indicate no flow instabilities, then operation under 1-g conditions will certainly be stable according to the Miles stability criteria.

Heat Transfer

It was pointed out in the Theory section of this report that the Nusselt number in the condensing annular flow model of Bae, et al. (ref. 16) was essentially inversely proportional to $\delta^{3/2}$ or δ^+ in the laminar sublayer. Consequently, as the film thickness approaches zero, $Nu \to \infty$, not surprisingly.

The experimental observations indicating an uneven liquid film thickness about the inner wall periphery led logically to the modified heat transfer model described in the previous section of this report. The principal result of this modified model was that a lower rate of heat transfer would occur under 0-g conditions

because of the greater average thermal resistance provided by a uniform thickness of condensate. This result assumed $\delta/D << 1$, which is not accurate at lower quality flows. Since annular, stratified-annular, or wavy-annular flow occurred over as much as 85 percent of the two-phase region, this approximation should be refined so as to accommodate that portion in which δ may be as large as $D/2$ at the tube bottom. That is, it is necessary to evaluate h_{1-g}/h_{0-g} as a function of the channel length (or equivalently, of the flow regime). Also, the actual variation of δ with angle θ should be included in refining the model. This dependence of δ upon θ would be a function of axial position also, and would additionally depend upon the wetting characteristics of the fluid.

While this model has been discussed relative to the annular flow pattern, it may be adaptable to the slug flow region as well, since the principal difference would be the presence of a pure liquid portion between each elongated bubble, for which the single phase heat transfer coefficient is easily calculated. Photographic observations indicated that the film thickness at the tube bottom in the slug flow or elongated-bubble regimes continues to increase gradually over that in the last stages of the annular-type flow regime.

In either the case of the Bae, et al. model and its predicting equations, or the extended modified model just discussed, comparative experimental measurements under 1- and 0-g conditions would be invaluable in testing their validity, thereby providing a reliable method for the heat transfer design of future systems.

CONCLUSIONS

The principal conclusions to be drawn from this combination experimental-analytical study are believed to be as follows.

The Baker flow-regime map appears to predict flow patterns in the present system reasonably well. At the same time, there are insufficient data points available for making more definitive conclusions.

Additional data, including zero-g data, should be compared further with Baker chart predictions and the flow regime map recently proposed by Soliman and Azer (ref. 31).

A very large fraction (at least 75 percent) of the flow in the quartz-tube system was in the annular, stratified-annular, or wavy-annular regimes, indicating that an annular-flow heat transfer model is quite reasonable.

Film thickness measurements and liquid and vapor velocity measurements strongly indicate that values of quality determined in previous ground-testing of the condensing system were consistently high--perhaps by as much as 30 percent in many cases.

A perfectly stable, smooth interface will not necessarily exist under 0-g conditions in an annular flow system, as predicted by classical wave-instability theory. Instead, wall curvature (as in small diameter systems) and liquid surface tension will tend to ensure a finite spacing between disturbances growing in the liquid film, which could conceivably lead to a transition to slug-flow in a 0-g environment also, under some flow conditions.

Disturbances in the annular film appear to be spaced at a distance close to the critical wavelength, modified to include the effects of wall curvature.

Parallel channel instabilities do not appear to present a problem in 0-g condensing systems, as determined by the Ledinegg criterion, since the system heat flux will be limited to modest values by the radiation heat transfer resistance.

Gravity-independent instabilities in annular flow, governed by the relative magnitudes of the Reynolds and Weber numbers, may occur under 0-g conditions. However, the horizontal testing of a refrigerant-12 system in a 1-g environment should provide a more extreme set of operating conditions with respect to this type of instability (leading to a slug-flow transition) than that existing in a 0-g environment.

A relatively smoother liquid-vapor interface should exist under 0-g operating conditions due to the absence of gravity-induced film distortions. This would lead to smaller pressure gradients and lower pressure drops than experienced under 1-g conditions. Again, testing under 1-g conditions should be more conservative.

Due to a smoother liquid-vapor interface, lowered interfacial shear stresses may result in a lowered rate of heat transfer (rate of condensation) in accordance with the Reynold's analogy. This effect would be in addition to possible adverse effects due to liquid redistribution about the channel wall in going from 1-g to 0-g conditions.

It appears that condensation heat transfer coefficients will be lower relative to that under 1-g conditions, largely because of the uniform redistribution of liquid about the channel wall. That is, the average heat transfer coefficient about the channel periphery associated with a uniform film thickness (0-g conditions) appears to be less than that existing for a non-uniform film thickness (1-g conditions), for the same void fraction.

RECOMMENDATIONS

The principal thrust of future investigations that is indicated by the present study is twofold--investigation of gravity-independent film instabilities in annular flow, and further analysis, development, and comparison of heat transfer models for flow condensation systems. The latter will be most obviously meaningful if reliable experimental results (1-g and 0-g) are available for testing the validity of the models. Regarding the type of experimentation that is desirable, the words which follow, taken from Collier (ref. 9) are believed by this author to be especially worthy of heeding. Though they are said with reference to boiling heat transfer systems, they appear equally valid for condensation heat transfer due to the many similarities between the two.

> . . . It is only in the last ten years that important contributions have been made towards understanding the processes involved in progressive vaporization along a tube. The lack of progress in the earlier work arises, in part, from the large number of experimental variables which are present but, in the main, it is the consequence of the fact that early workers in the field reported only effects on the performance of the evaporator resulting from independent variables altered by the operator. It is clear. . .that it is essential to study the local or point conditions in the evaporation. No such study was published prior to 1952.

With the preceding in mind the following recommendations are offered:

1. Establish the validity of the Miles stability criteria relative to gravity-independent film instabilities in annular flow by means of measurements obtained from basic (rather than operational) flow condensation experiments conducted under 1-g and 0-g conditions.

2. Expand upon and continue the development of the two-phase heat transfer model which has been presented herein in fundamental form, so as to permit accurate prediction of 0-g heat transfer performance, based upon 1-g test results.

Specifically, further work should include a parametric study of model modifications (necessitated by liquid film redistribution) throughout the annular, slug, and elongated-bubble flow regimes. One of the parameters investigated must be the magnitude of the liquid film thickness at the top of the channel; consequently, liquid-solid wetting characteristics must be considered.

3. Incorporate the expansion and modifications recommended in 2 above into the heat transfer models of (a) Collier and Pulling (ref. 35); (b) Dengler and Addoms (ref. 36); (c) Guerrieri and Talty (ref. 37); and (d) Chen (ref. 38) (see Appendix B for further discussion of these models).

4. All of the preceding models have been developed for boiling and evaporating annular flow systems; hence their applicability in a flow condensation system should be verified with experimental results of 1-g and 0-g tests.

5. Compare the heat transfer predictions of the Bae model with 1-g and 0-g tests.

APPENDIX A

TYPES OF INSTABILITY

The types of instabilities that characterize flow condensation systems may be broadly classified into the following three categories:

1. Interface instability
2. Film instability
3. Flow instability

These instabilities may be thought of as being controlled by various dimensionless ratios of surface tension, inertial, viscous, and gravitational forces. Thus, stability criteria for each of the three preceding categories may be established in terms of the dimensionless quantities characterizing each situation.

Reference 11 contains a comprehensive investigation of the various types of instability that may occur in a condensing system under normal and reduced gravity fields. It is concluded therein that the only kind of instability that may result in fluctuation in condenser flow, pressure, etc., is that due to runback of the condensate film. Although the remainder of this section will be devoted to runback instability, the several other types of instabilities will be discussed in the following sections.

Liquid runback instability in an upward flow, annular condensing system consists simply of a folding back or run-back of the liquid film due to gravitational forces. This gravity-induced instability may be classified as a Rayleigh-Taylor type instability. Relative to the condensing system under study, this type of instability would not be expected to appear under a near-zero gravity environment. However, if spacecraft acceleration occurs, such that an artificial gravity field is induced, the axial component of the gravitational force could lead to a runback instability.

It would be expected that such an instability may develop when the gravitational forces acting on the liquid film become comparable to the viscous shear forces acting on the interface of the annular liquid film.

The relative magnitudes of these forces may be estimated by forming the ratio of the Froude and Reynolds numbers. Since

$$Fr = \frac{\rho_\ell (V_\ell)^2}{(\rho_\ell - \rho_g) a \delta} \quad \alpha \quad \frac{\text{inertial forces}}{\text{gravitational forces}} \tag{A-1}$$

and

$$Re = \frac{\rho_\ell V_\ell \delta}{\mu_\ell} \quad \alpha \quad \frac{\text{inertial forces}}{\text{viscous forces}} \tag{A-2}$$

the ratio of Fr to Re yields

$$\frac{Fr}{Re} = \frac{\mu_\ell V_\ell}{(\rho_\ell - \rho_g) a \delta^2} \quad \alpha \quad \frac{\text{viscous forces}}{\text{gravitational forces}} \tag{A-3}$$

When the ratio Fr/Re is unity, the viscous and gravitational forces are comparable and liquid runback instability may occur. Equation (A-3) provides a means of estimating when runback may occur, providing the film thickness δ may be measured or otherwise determined.

Interface Instability

At some axial position near the end of a condenser tube the vapor phase is completely condensed, forming a liquid-vapor interface across the tube. The liquid then becomes further subcooled as it approaches the tube end. It is possible that the interface may oscillate due to external or internal disturbances of the system. Also, impacting drops or gravitational forces may distort the interface itself. In any event, distortions or disturbances of the interface could lead to vapor slugs or bubbles leaving the condenser tube, eventually entering the compressor and resulting in severe cavitational type damage to the compressor. It is thus

desirable to understand the conditions that may lead to instability of the interface so that such damage or failure of the system may be avoided.

a. Meniscus Instability. To insure "static" stability of the interface the condenser tube diameter should be smaller than the critical diameter. The critical diameter is defined as the maximum diameter tube that retains liquid when inverted and subjected to internal and external perturbations. An expression for the critical diameter for either wetting or non-wetting liquids is given by reference 19:

$$D = 1.835 \sqrt{\frac{\sigma}{(\rho_\ell - \rho_g)\frac{g}{g_c}}} \qquad \text{(A-4)}$$

It is seen that a reduction in local gravitational field indicates a larger critical diameter, indicating that the 1-g environment is more severe with respect to static equilibrium of the interface. This type of instability should not be expected, then, if the system is designed for a 1-g field and is then subjected to a low gravity environment.

The dimensionless parameters characterizing the meniscus are the Bond number (Bo) and the Weber number (We), where

$$\text{We} \;\alpha\; \frac{\text{inertia forces}}{\text{surface tension forces}}$$

$$\text{Bo} \;\alpha\; \frac{\text{gravity forces}}{\text{surface tension forces}} \qquad \text{(A-5)}$$

The relative importance of the inertia, gravity, or capillary forces that govern meniscus dynamics is shown graphically in reference 11.

From the differential equations describing the meniscus shape the onset of instability appears related to a critical Bond number that is apparently independent of contact angle and gravitational

environment. Experimental results of Masica (refs. 39 and 40), obtained in normal and reduced gravity fields, indicate a critical Bond number based on tube radius of 0.84, when the acceleration is parallel to the tube axis. For acceleration normal to the tube axis different critical Bond numbers were found, and are shown graphically in reference 11.

b. Interfacial Instability Due to Slug Flow. The origin of slug flow is similar to that producing droplet entrainment in the vapor core. In slug flow vapor shear forces acting on the liquid annulus may tear from the liquid film a sufficiently large mass of liquid from opposite sides of the tube to completely bridge the tube diameter, producing a pattern of vapor slugs separated by a thickness of liquid. This is illustrated by the figure below.

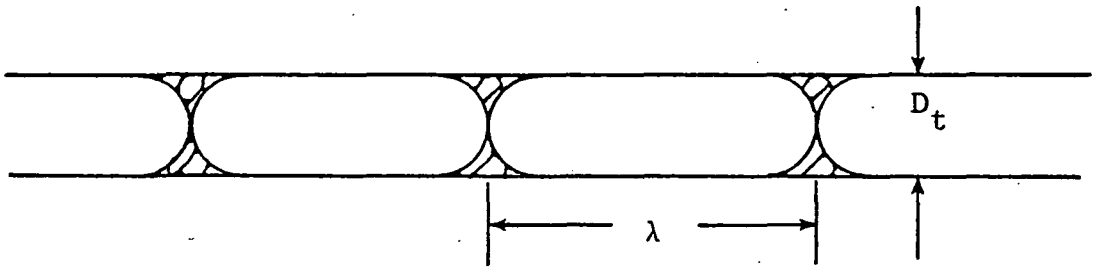

Figure A-1. Griffith and Lee (ref. 41) plug flow geometry.

As in the case of the liquid drops, arrival of these liquid-vapor slugs at the interface could produce fluctuations in the interface location, leading to fluctuations in pressure, perhaps system instability, and possibly escape of vapor from the condenser into the compressor. To predict slug flow effects one should perhaps begin by determining the conditions under which the transition from annular to plug flow occurs.

Griffith and Lee's (ref. 41) predictions of this transition, which have been substantiated by experimental results, assume a model in which the liquid bridging occurs at a spacing equal to

the most unstable film wavelength, λ_c. The liquid volume fraction in a tube volume having a length λ_c is

$$R_\ell = \frac{D}{3\lambda_c}$$

Assuming zero slip, the relation between quality and liquid volume fraction is

$$x = \frac{1}{1 + \frac{R_\ell}{(1 - R_\ell)} \frac{\rho_\ell}{\rho_v}} \qquad \text{(A-6)}$$

The preceding equations permit calculation of the quality at which transition occurs, provided that one knows (or calculates) λ_c.

Using a "most unstable wavelength" value of 4.5D, and assuming a density ratio of 2450, a transition quality of 0.5 percent is calculated in reference 11. The plug flow region is calculated to cover 0.45 percent of the tube length, assuming a liquid leg covering 10 percent of the tube length. Since the liquid separating the vapor plugs occupies a tube length of one-third the tube diameter, it is concluded that the interface will oscillate no more than one-third of a tube diameter. This conclusion apparently ignores the movement that may be caused by the moving liquid "bridge" as it strikes the interface, such as that considered for entrained liquid drops traveling in the vapor core.

Two other considerations should also be pointed out. The first is that the critical wavelength λ_c is a function of $\frac{1}{g}$, so that a reduction in gravitational field should produce a much larger wavelength. According to the Griffith-Lee model the spacing between liquid slugs would be increased, resulting perhaps in lower frequency pressure oscillations in the system and a comparable effect on the movement of the interface.

The second consideration concerns the quality at which transition to plug flow occurs. As mentioned earlier, for a case of liquid-vapor

density ratio of 2450 the transition is calculated to occur at 0.5 percent quality--a position close to the interface. However, in a condensing freon system for the conditions expected in the present application the density ratio is substantially lower-- $\rho_\ell/\rho_v \approx 11$. Consequently, the quality at which transition occurs is much higher, as indicated by equation (A-6), and the length of tube over which a plug flow regime exists is likely to be considered larger.

. Film Stability

a. Surface Wave Instabilities. Wave formation on the condensing liquid film may arise from instabilities of basically two different origins--Tollmein-Schlichting and Kelvin-Helmholtz instabilities. The former is associated with a liquid film undergoing transition from laminar to turbulent flow. The latter is associated with instabilities at the interface of layers of fluid undergoing relative motion.

A third type of instability, a Rayleigh-Taylor instability, may occur in a system of two layers of fluids of different density which has an acceleration vector directed from the more dense to the less dense phase. In reduced gravity fields where the acceleration vector is very small, this type of instability would not be expected to be of significance. In an earth environment, however, this type of instability may well be of consequence. With respect to Rayleigh-Taylor instabilities, then, condensing in a 1-g environment should provide a more severe test than a 0-g environment.

Elaborating on the Kelvin-Helmholtz instability, the appropriate stability criterion parameter, representing the ratio of buoyancy to inertia forces, is

$$\frac{g\,(\alpha_1 - \alpha_2)}{\alpha_1\alpha_2\,\,(u_v - u_\ell)^2} \qquad \text{(A-7)}$$

where g = acceleration of gravity

α_1, α_2 = density ratios, $\rho_\ell/(\rho_\ell - \rho_v)$ and $\rho_v/(\rho_\ell + \rho_v)$

u_v, u_ℓ = fluid velocities.

Physically, this parameter may be thought of as reflecting the tendency of the fluids toward mixing, being prompted by high inertial forces and retarded by surface tension forces.

b. Film Runback Instability. Runback of the liquid film will occur when gravitational forces oppose and become more dominant than the wall shear forces. Condensing in an upward position will result in substantial perturbation of the system flow parameters, although, surprisingly, this type of instability has also been observed in downward condensing systems. This type of instability may be classified as a Rayleigh-Taylor type instability.

A simple criterion for determining the vapor quality at which runback occurs may be obtained by making a force balance (acceleration and shear forces) on an element of the liquid film, relating film height to void fraction, and setting the wall shear stress to zero at the location where runback occurs. This analysis assumes that pressure and momentum forces are negligible. Also, the condensing liquid film is assumed to be of a boundary layer nature. The resulting expression is

$$\frac{xG_T}{\alpha\rho_v} = \frac{a\rho_\ell}{2\mu_e}\frac{D^2}{4}\left(1 - 2\,\alpha^{1/2} + \alpha\right) \qquad \text{(A-8)}$$

If the void fraction may be related to quality by

$$\alpha = \frac{1}{1 + \left(\frac{1-x}{x}\right)\left(\frac{\rho_v}{\rho_\ell}\right)^{2/3}} \qquad \text{(A-9)}$$

the quality at which the wall shear goes to zero may be calculated by a trial and error procedure. This technique was used in reference

11 in application to a SNAP-50/SPUR radiator condenser. Their calculations for a system condensing vertically upward showed that runback occurred very nearly at the interface. Once again, however, the liquid/vapor density ratio was much larger than that characterizing freon refrigerants, so that in the present application liquid runback may occur at a much higher quality.

Factors which have not been taken into account in equation (A-8) are the restoring forces of liquid surface tension, vapor friction and momentum exchange. In the absence of the inclusion of restoring forces, however, equation (A-8) should be a conservative criterion.

Another approach in establishing a stability criterion is to develop an expression for the ratio of shear forces to gravity forces in the liquid film and then evaluate this ratio for condensing systems that have already been built and tested. This approach, however, still ignores the restoring forces discussed earlier, which may vary from system to system. Nevertheless, the expression derived in reference 11 is

$$\frac{Fr_f}{Re_f} = \frac{\tau_{vap}}{\delta\ \rho_\ell\ \frac{a}{g_c}} = \frac{1}{2} + \frac{16}{\pi}\ \frac{\mu_\ell}{\rho_\ell\ \rho_v}\ \frac{xW_T}{a\ D^4\ (\alpha - 2\alpha^{3/2} + \alpha^2)} \qquad \text{(A-10)}$$

This force ratio may be referred to as the liquid runback parameter. Physically, it provides a measure of the sensitivity of the annular film to an axial acceleration field.

In low or zero gravity fields it is not expected that liquid runback instability will affect system operation significantly. In a low gravity environment (10^{-3} to 10^{-7} g) the restoring surface tension forces of the film will override the disruptive gravitational forces. If runback does occur, equation (A-8) indicates it should occur at a very low quality in a low gravity environment.

Flow Instability

a. Aperiodic Instability. For two-phase flow systems with heat transfer the Ledinegg criterion states that the necessary condition for flow stability (or the absence of an aperiodic instability) is that $\partial(\Delta P)/\partial G < 0$. Considering pressure drops in the inlet and exit manifolds, that due to friction in the tube, and pressure rises due to momentum recovery and the length of the liquid leg, and assuming a constant heat flux over the tube length, the heat flux necessary to produce a negative pressure drop gradient is

$$\frac{q}{A} < \frac{\frac{3}{4} G_T^2 \frac{f_v h_{\ell v}}{\rho_v} + \frac{a \rho_\ell D h_{\ell v}}{4}}{G_T/\rho_v} \qquad \text{(A-11)}$$

This represents a heat flux of large magnitude--sufficiently large that this type of instability should not occur in a radiating condenser system.

b. Periodic Instabilities. For systems having several parallel flow channels an instability in a single channel, due perhaps to a change in flow regime, will not appreciably affect the overall pressure drop of the system, but will produce a flow redistribution among the other channels, affecting the heat transfer occurring in the system at the same time. This thermal and hydrodynamic coupling, combined with a potential for positive feedback, may lead to sustained oscillations and a resonant type condition. The subject of flow oscillations is not fully understood or predictable.

APPENDIX B

FLOW CONDENSATION HEAT TRANSFER MODEL

A simple model of flow condensation in a horizontal tube may be based upon the annular flow pattern, as indicated in figure B-1. In an actual system, resistance to heat transfer will exist in the tube wall and at the outer surface of the tube in the form of a radiative or convective resistance.

In the present test program it was desired to calculate quantities such as (a) length required for complete condensation, (b) quality, (c) void fraction, and (d) film thickness.

If vapor enters the condenser at superheated conditions the local quality is given by

$$x = x_o - \frac{\int_o^L q \, \pi \, D \, dL}{W_T \left[h_{fg} + c_p \, (T_{sup} - T_{sat}) \right]} \qquad \text{(B-1)}$$

where x_o may be determined from temperature and pressure measurements. The heat flux must be calculated, and may be variable over the channel length. The local heat flux is given by

$$q = U \, A \, (T_w - T_f) \qquad \text{(B-2)}$$

where

$$\frac{1}{U} = \frac{tD}{k_w \, (D + t)} + \frac{1}{h_c} + \frac{1}{h_{ow}} \, \frac{D}{(D + 2t)}$$

For the single phase regions (liquid or vapor) one may evaluate h from the familiar expression for turbulent flow,

$$\frac{hD}{k} = 0.023 \left(\frac{DV}{\nu} \right)^{0.8} \left(\frac{c_p \mu}{k} \right) \left(\frac{\mu_m}{\mu_w} \right)^{0.14}$$

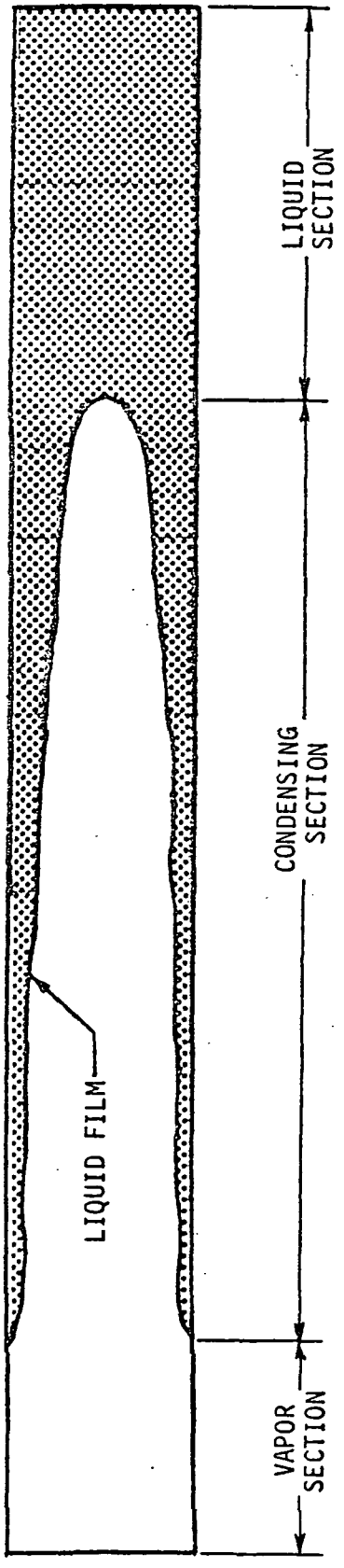

Figure B-1. Annular condensing flow pattern.

The condensing heat transfer coefficient is not as easily calculated. (However, condensing heat transfer coefficients are so large, typically, that the overall contribution to thermal resistance is very small.) An estimate of h_c may be obtained from equations (57a) and (57b). However, it should be observed that these equations, recommended by Hewitt (ref. 30) for application to annular two-phase flow, were based upon results obtained in boiling and vaporization systems, rather than condensation systems. Justification for use here in condensation systems is that nucleate boiling typically does not occur in a thin-film annular flow system. Hence the lack of a nucleation type heat transfer mechanism in flow condensation systems is comparable to the liquid vaporization and absence of nucleation existing in annular flow systems with heat addition. In fact, each of the three versions of equation (57a) recommend using modified equations if nucleate boiling does occur in the liquid film.

The correlations proposed by Dengler and Addoms, Guerreri and Talty, and Collier and Pulling (see equation 57b) can be improved upon by the correlation proposed by Chen (ref. 38). The average percentage deviations of data correlated by the former three correlations ranges from about 30 to 40 percent, while the deviation with the Chen correlation is only about 10 percent. Chen introduces a flow parameter F and a suppression factor S that were determined empirically. Because of the vast improvement in accuracy provided by the Chen correlation further investigation may be desirable. The calculational procedures are more complex, however, requiring eight separate steps and obtaining values of F and S from two graphs (see ref. 9).

Another alternative for evaluating h_c is to use a Nusselt equation for condensation on the outside of a horizontal tube, but modified to account for the stratified layer of liquid tending to accummulate at the bottom of the tube, as described in reference 9, pp. 328-333. This modification would best approximate the type

of flow pattern observed, though the modification is based upon a condensate film of "negligible" thickness. Additionally, adapting the stratified flow modification to the zero-g flow pattern of a uniformly thick annular film appears inconsistent with one of the assumptions of the model, i.e., that the rate of condensation on the stratified layer is negligible. In a zero-g environment, this would be tantamount to saying that the condensation rate about the entire tube periphery is negligible.

Having evaluated the single phase and two-phase heat transfer coefficients, the wall resistance and the external resistance (convective and/or radiative), the heat flux may be calculated and the quality variation may then be determined. The void fraction may then be calculated from Zivi's equation, equation (48), and the film thickness obtained from the expression

$$\delta = \frac{D}{\alpha + 1}$$

which is valid for a thin film annular flow model.

The preceding procedure is general in that the heat flux, and quality need not be uniform over the tube length. It is at the same time an iterative procedure, since the two-phase friction multiplier used in equation (57a) is a function of quality, whereas the quality is unknown at that point in the calculational procedures.

The methods described herein have been used to calculate and compare condensation lengths in the present experimental system (ref. 29). The agreement obtained was accurate to within ± 20 percent, and judged to be usable with confidence to predict test results and analyze test data. It should be pointed out that the prediction of condensation length per se is actually relatively insensitive to the predicted values of the condensing coefficient, since the thermal resistance provided by the condensing film is so much smaller than either the wall thickness or the external resistance. The question of which correlation best

predicts condensation heat transfer coefficient cannot be resolved by these predictions of condensation lengths. Instead, this must be accomplished by fundamental studies of the flow condensation process.

REFERENCES

1. "Development of a Direct Condensing Radiator for Use in a Spacecraft Vapor Compression Refrigeration System," J.L. Williams, E.G. Keshock and C. Wiggins, ASME Trans., Jnl. of Engr. for Industry, V. 5, No. 4, Nov. 1973.

2. "An Experimental Study of Flow Condensation Phenomena Under Zero-Gravity Conditions in a Space Radiator System," E.G. Keshock, J.L. Williams, G. Spencer and B. French, Proc. of Fifth Int'l. Ht. Tr. Conf., V. III, Tokyo, 1974.

3. Zero-G Radiator/Condenser Experiment Package Test, J.L. Williams and W.A. Whitten, Vought Systems Division, Dallas, TX, Rept. No. VSD T122-RP-020, Feb. 14, 1973.

4. "Performance of Boiling and Condensing Equipment Under Simulated Outer Space Conditions," C. Feldmanis, ASD-TDR-63-862, Wright-Patterson AFB, Nov. 1963.

5. "Experimental Pressure-Drop Investigation of Non-Wetting, Condensing Flow of Mercury Vapor in a Constant Diameter Tube in 1-g and Zero-Gravity Environments," J.A. Albers and R.P. Macosko, NASA TN D-2838, June 1965.

6. "Photographic Study of Condensing Mercury Flow in 0 and 1-g Environments," D. Namkoong, et al., NASA TN D-4023, June 1967.

7. "Flow Stability and Gravitational Effects in Condenser Tubes," M. Soliman and P.J. Berenson, Proc. Int'l Ht. Tr. Conf., Paris, 1969.

8. "Study of Wetting and Non-Wetting Mercury Condensing Pressure Drops," A. Koestel, et al., NASA TN D-2514, Nov. 1964.

9. Convective Boiling and Condensation, John G. Collier, McGraw-Hill Book Co. (UK) Ltd., 1972.

10. "Two-Phase Flow Heat Transfer," P. Griffith and L.S. Tong, AIChE Today Series, 1973.

11. Analysis, Criteria Development, and Design of an Orbital Condensing Heat Transfer Experiment, Airesearch Mfg. Div., Los Angeles, Fin. Tech. Rept., Contr. No. NAS8-21005.

12. "Two-Phase Two-Component Flow in the Viscous Region," R.C. Martinelli, J.A. Putnam and R.W. Lockhart, Trans. AIChE, V. 42, 1946, p. 681.

13. "Prediction of Pressure Drop During Forced Circulation Boiling of Water," R.C. Martinelli and D.B. Nelson, Trans. ASME, V. 170, 1948, p. 695.

14. The Effect of Vapor Velocity on Condensation Inside Tubes, F.S. Carpenter and A.P. Colburn, Proc. of Gen. Discussion of Ht. Tr., Inst. of Mech. Engrs. and ASME, July 1951, pp. 20-26.

15. One-Dimensional Two-Phase Flow, G.B. Wallis, McGraw-Hill Book Co., NY, 1969.

16. Refrigerant Forced Convection Condensation Inside Horizontal Tubes, S. Bae, J.S. Maulbetsch and W.M. Rohsenow, Rept. No. DSR 72591-71, Contr. No. ASHRAE RP 63, M.I.T., Cambridge, MA, Dec. 1, 1970.

17. Development of a Refrigeration System for Lunar Surface and Spacecraft Application," C.L. Wiggins, Vought Missiles and Space Co., Dallas, TX, Rept. No. T122 RP 09, Contr. No. NAS9-9912, Feb. 15, 1972.

18. "The Hydrodynamic Stability of a Thin Film of Liquid in Uniform Shearing Motion," J.W. Miles, Jnl. of Fl. Mech., 1960.

19. Space Radiator Study, R.J. Dennington, ASD-TDR-61-697, Oct. 1963.

20. Instability of Flow During Natural and Forced Circulation, M. Ledinegg, USAEC Rept. AEC-TR-1861, Translated from Die Warme, No. 61, 1938.

21. "Development of a Direct Condensing Radiator for Use in a Spacecraft Vapor Compression Refrigeration System," J.L. Williams, E.G. Keshock and C. Wiggins, ASME Trans., Jnl. Of Engr. for Industry, V. 5, No. 4, Nov. 1973.

22. Zero-G Radiator/Condenser Experiment, B.O. French and G.L. Spencer, Doc. No. GSD-SH-024, Crew Systems Division, Johnson Space Ctr., Houston, TX, March 29, 1974.

23. Zero-G Radiator/Condenser Test Report, G. Spencer and B.O. French, CSO-JSC, Sept. 1, 1973.

24. "Design of Pipe-Line for the Simultaneous Flow of Oil and Gas," O. Baker, The Oil and Gas Journal, July 26, 1954.

25. Nuclear Heat Transport, M.M. El-Wakil, International Textbook Co., 1971.

26. Nucleate and Film Boiling in Reduced Gravity from Horizontal and Vertical Wires, R. Siegel and E.G. Keshock, NASA TR R-216, Feb. 1965.

27. Heat Pipe Investigations, J.P. Marshburn, NASA TN D-7219, Aug. 1973.

28. "The Hydrodynamic Stability of a Thin Film of Liquid in Uniform Shearing Motion," J.W. Miles, Jnl. of Fl. Mech., 1960.

29. Validation of a Freon-12 Condenser Computer Program, D.W. Cook, Tech. Memorandum, Proj. No. 3705, Lockheed Elec. Co. Inc., Houston, TX, June 1973.

30. Annular Two-Phase Flow, G.F. Hewitt and N.S. Hall-Taylor, Pergamon Press, 1970.

31. "Visual Studies of Flow Patterns During Condensation Inside Horizontal Tubes," H.M. Soliman and N.Z. Azer, Paper Cs 1.6, Fifth Int. Ht. Tr. Conf., Vol. III, Tokyo, September 1974.

32. Void Fractions in Two-Phase Flow: A Correlation Based Upon an Equal Velocity Head Model, S.L. Smith, Inst. of Mech. Engg., Vol. 184, London, 1969-70.

33. Personal communication, G. Spencer, Johnson Space Center, NASA, July 1974.

34. "The Hydrodynamic Crisis in Pool Boiling of Saturated and Subcooled Liquid," N. Zuber, M. Tribus, and J.W. Westwater, Int. Dev. in Ht. Tr., Pt. II, ASME, pp. 230-236, 1961.

35. "Heat Transfer to Two-Phase Gas-Liquid Systems," J.C. Collier and D.J. Pulling, AERE-R 3809, 1962.

36. "Heat Transfer Mechanism for Vaporization of Water in a Vertical Tube," C.E. Dengler and J.N. Addoms, Chem. Engr. Prog. Symp. Series, Vol. 52, No. 18, pp. 95-103, 1956.

37. "A Study of Heat Transfer to Organic Liquids in Single Tube, Natural Circulation Vertical Tube Boilers," S.A. Guerrieri and R.D. Talty, Chem. Engr. Prog. Symp. Series: Heat Trasnfer, Vol. 52, No. 18, pp. 69-77, 1956.

38. "A Correlation for Boiling Heat Transfer to Saturated Fluids in Convective Flow," J.C. Chen, ASME Sixth Nat'l. Ht. Tr. Conf., ASME preprint 63-HT-34, Boston, Aug. 11-14, 1963.

39. Hydrostatic Stability of the Fluid-Vapor Interface in a Gravitational Field, W.J. Masica, D.A. Petrash, and E.W. Otto, NASA TN D-2267, 1964.

40. Hydrostatic Stability of the Liquid-Vapor Interface in a Low-Acceleration Field, W.J. Masica, J.D. Derbul, and D.A. Petrash, NASA TN D-2444, 1964.

41. The Stability of an Annulus of Liquid in a Tube, P. Griffith and K.S. Lee, ASME Paper No. 63-WA-97, 1963.

42. Fundamentals of Low Gravity Phenomena Relative to Fluid System Design, P.J. Berenson, AiResearch Mfg. Co., Los Angeles, CA.